UNIVERSITA' POLITECNICA DELLE MARCHE

FACOLTA' DI INGEGNERIA

Master of Science Course in Environmental Engineering

Hydrodynamic investigation of Pioraco alluvial valley as support

for geotechnical modeling of consolidation processes

Advisor: Student:

Prof. Elisa Mammoliti   Cristiano Galeotti

Co-advisors:

Prof. Alberto Tazioli

Dr. Davide Fronzi

A.Y. 2021 / 2022

Summary

Riassunto

Questo studio di tesi è volto alla determinazione di un modello concettuale di carattere idrogeologico della pianura alluvionale di Pioraco (Regione Marche, Italia), avvalendosi di dati di letteratura e dati derivanti da una campagna indagini in-situ. Il paese di Pioraco è interessato da fenomeni di consolidazione dello strato di argille presenti in corrispondenza del quartiere 'La Madonnetta' che ha causato l'abbassamento del suolo e cedimenti degli edifici sovrastanti. La definizione del modello è stata ottenuta a partire da un'accurata ricerca di letteratura riguardo le condizioni idrogeologiche dell'area di studio, supportata da attività di campo per la misurazione diretta del livello piezometrico nel tempo e l'esecuzione di test con traccianti artificiali. Il modello concettuale è stato integrato da un'accurata ricostruzione stratigrafica ottenuta attraverso i sondaggi stratigrafici disponibili. L'analisi ha evidenziato la presenza di una spessa coltre di materiale alluvionale a natura argillosa al di sopra di materiale conglomeratico/ghiaioso il quale costituisce un orizzonte ad alta permeabilità che permette la filtrazione d'acqua sotto elevati gradienti idraulici. L'innesco di tali gradienti è stato attribuito e verificato, tramite realizzazione di mappe piezometriche dal 2004 al 2022, alle operazioni di pompaggio d'acqua in falda iniziate nel 2009 ed interrotte nel 2018 in seguito a fenomeni di instabilità in corrispondenza del pozzo di alimentazione. Infine, è stata effettuata un'analisi delle precipitazioni volta a determinare la possibile relazione tra oscillazioni della superficie piezometrica e l'abbassamento della superficie topografica. La valutazione di parametri come permeabilità e le direzioni di flusso, determinati tramite misurazioni dirette e test in-situ, costituisce una risorsa fondamentale per la costruzione di modelli geotecnici non svincolati dal contesto idrogeologico dell'area di studio e per pianificare adeguate strategie di pianificazione territoriale.

Abstract

The aim of this thesis is to construct a hydrogeological conceptual model of the alluvial valley of Pioraco (Marche Region, central Italy), integrating data from the literature with data derived from *in-situ* surveys. Pioraco village is affected by the process of consolidation of the clay layer in correspondence of the Madonnetta district which has caused the soil subsidence and the failure of buildings. The definition of this model has been achieved through a literature review about the hydrogeological condition, supported by *in-situ* surveys such as the measurement of piezometric levels and the tracer testing. The conceptual model was integrated by an accurate stratigraphic reconstruction based on the available stratigraphic boreholes. The analysis has revealed a thick layer of clayey alluvial deposits lying on the top of alluvial and slope deposits gravel materials. The last one constitutes a high permeability medium able to accommodate the water drainage under elevated hydraulic gradients. The hydraulic gradient magnitude has been intensified by the water pumping operation started in 2009 and verified through piezometric maps realisation along the period 2004-2022. Finally, an accurate analysis of the precipitations is proposed to determine the possible relationship between piezometric surface oscillation and the soil subsidence. The determination of parameters of permeability and water flux directions, calculated through direct measurements and in-situ tests, constitute a solid support to build up a geotechnical model bonded to the hydrogeological condition of the study area and permit to develop the correct strategies for the land use planning and buildings reconstruction.

1. Introduction

Land subsidence is the gentle settling or rapid sinking of the discrete segments of the ground surface due to the consolidation of sediments and thus, subsurface movement of earth materials because of increasing effective stress (Galloway and Burbey, 2011; Ma et al., 2018). The term subsidence refers to a surface point sinking to a lower level and can include a structure settling into the ground or the ground itself lowering and carrying the structure with it (Reddish & Whittaker, 2012).

In the last 25 years, the Pioraco village (Marche Region, central Italy) has been subjected to the soil subsidence and the associated buildings settlement. This study presents an investigation of the principal causes which may be related to consolidation processes in the alluvial plain of Pioraco, with the purpose to build up a solid conceptual model useful for the geotechnical evaluations. The adopted approach consists in combining several engineering fields: a) the first one investigating the hydrogeological background of the area through a literature review, then performing field surveys to measure the permeability; 2) the latter integrating the analysis of the precipitation in order to understand the recharge mechanisms of the aquifer. Soil properties influence the settlement, especially the intrinsic consolidation characteristics and the external stresses. Ground subsidence can be triggered by several geological factors or climatic processes, anyway human-induced land subsidence cases are 76.9% of all the subsidence cases around the world (Bagheri-Gavkosh et al., 2021). The subsidence is frequently linked to intense faulting and opening of fissures in urban areas, generating a significant geologic hazard that needs to be accurately assessed and monitored (Brunori et al., 2015). Underground excavations (e.g., mining and tunnelling) and new settlements on the ground surface are likely the most common anthropogenic factors causing local scale subsidence (Guéguen et al., 2009, Jung et al., 2007, Samsonov et al., 2013). A the same time, fluid and gas exploitation are commonly associated with regional scale subsidence involving square kilometre areas (Dixon et al., 2006, Meckel et al., 2006, Teatini et al., 2011). Groundwater exploitation is likely the most challenging process as it generally affects large cities that require huge quantities of water for human activities (Bozzano et al., 2015). The evaluation of deformations in civil infrastructures or natural environments is normally assessed by the realization of fully accurate three-dimensional models by means of a range of complementary geomatics techniques such as total stations, global navigation satellite

systems (GNSS), photogrammetry, laser scanning (Di Stefano et al., 2022). Obtaining information on ground or building displacement is a key feature for performing detailed and quantitative evaluations of the state of subsidence processes, but additional studies concerning the geological, geotechnical and hydrogeological features of the area are necessary to gain a comprehensive knowledge of the mechanism controlling such processes, especially for the purposes of prediction and assessment of future expected events (Bozzano et al., 2015).

Bozzano et al. (2015) have demonstrated how the spatial pattern and deformation rate change is attributed to the fluctuations of the groundwater levels and the distribution and thickness of recent compressible deposits. Specifically, it was derived that the groundwater level variations drive the timing of subsidence triggering over the area, whereas the local geological conditions control the magnitude of the deformation process. More in detail, multi-layered aquifer settings including deep confined aquifers and the thick compressible clay layers present in many geological and hydrogeological conditions, facilitate the land subsidence development (e.g., Guo et al., 2015, Wang et al., 2019). For this reason, the combination of geological and hydrogeological modelling calibrated on piezometric dataset is essential to explain the spatial and temporal evolution of subsidence processes (Bozzano et al., 2015).

Therefore, carrying out a geotechnical model of consolidation processes, if not supported by geological and hydrogeological investigation, leads to a misleading conceptual model and erroneous predictions. Monitoring actions are necessary to guarantee health and safety conditions by controlling the evolution of deformation patterns or detecting significant instabilities. Laser Scanning (LS) and Close-Range Photogrammetry (CRP) are state of the art techniques for acquiring dense and precise topographic data at the output detail, for accurate volume measurements or modeling (Di Stefano et al., 2022).

2. State of the art

This chapter provides a detailed review of the literature (including technical reports) that will be addressed in the thesis work.

2.1 The consolidation process in Pioraco village

The Madonnetta district (Municipality of Pioraco, Italy) was built in the 1960-70s. This district extends for an area of approximately 24,000 m^2 and was built partly on the alluvial silty deposits (about 50 m of total thickness). The buildings were constructed of reinforced concrete and the elevations range from 2 to 5 floors. The area has been affected by several seismic events during the years and, after the 2016-2017 seismic events, the municipality of Pioraco was included in the list of municipalities of the seismic crater (defined by Civil Protection of Italy). Figure 1 shows the contour lines of the Madonnetta district that have been used as base to evaluate the vertical displacements of the soil.

Figure 1. Site plan of the area of interest; contour lines are shown in yellow (modified from Di Stefano et al., 2022).

In Pioraco village (Marche Region, Central Italy), the Madonnetta district has always been affected by land subsidence, causing strong damages to foundation of buildings and infrastructures (Figure 2) (Lenci, 2021).

Figure 2. Effects of land subsidence processes on the buildings of the Madonnetta district of Pioraco, July 2022.

When the Umbria-Marche region was strucked by the earthquake of 1997, the Madonnetta district started experiencing more severe buildings settlement as result of the variation of hydrologic scheme and the consequent drop of piezometric level in the area, that is responsible of the subsidence acceleration rate (Lenci, 2021). The clay deposit that stands below the district has been classified as inorganic clay of elevated plasticity and weak mechanical characteristics, subjected to consolidation process under its own weight (Lenci, 2021). After the earthquake of 1997, the Pioraco Municipality promoted a monitoring campaign of piezometric level variation and structures settlements rate through a high precision topographic levelling on datum points installed on buildings.

A geotechnical campaign was set up in 2020 by the "Struttura Commissariale per la Ricostruzione". The purpose was investigating the stratigraphy, determining the piezometric level in the study area and characterizing the hydraulic, mechanic and seismic features of the clay deposit. The study was integrated with several surveys necessary to implement direct

measures and collect soil samples. Laboratory tests on samples have confirmed the mechanical weakness of the material and the high compressibility degree (Lenci, 2021) which promote the settling. In addition, the results obtained from this geotechnical investigation permitted to determine fundamental parameters for the modelling of hydraulic and mechanic behaviour of the clay layer. The modelling was performed along two perpendicular sections passing across the centre of the Madonnetta district (Figure 3).
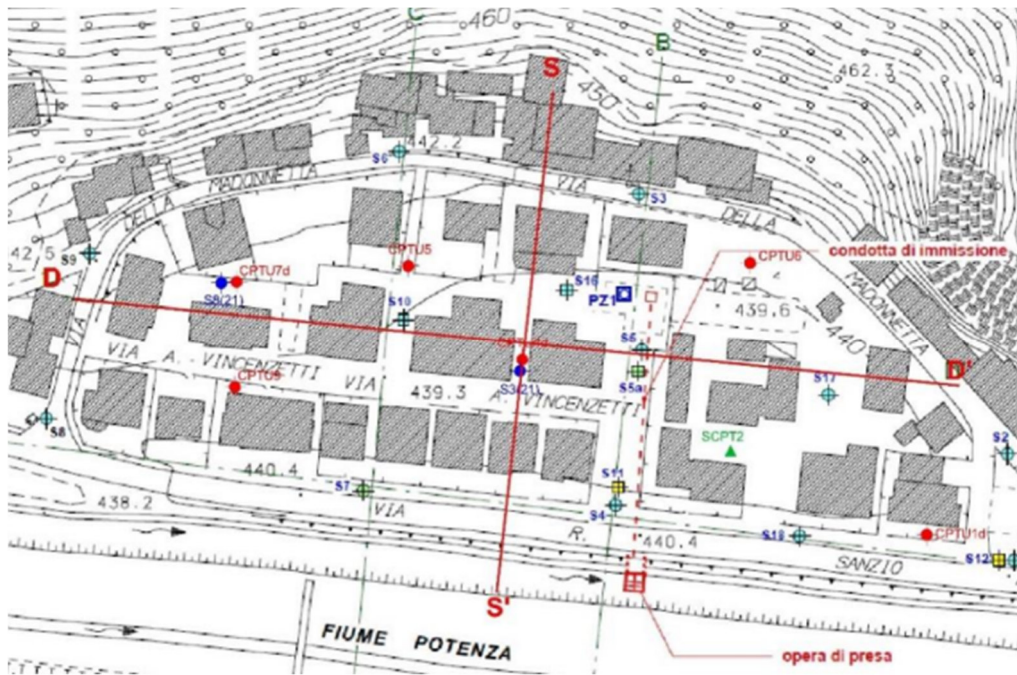

Figure 3. Sections for geotechnical modeling of consolidation processes (modified from Lenci, 2021).

Thanks to the modelling, it was possible to provide the consolidation predictions for the next 50 years. The model was developed using the finite elements method and considering the piezometer level variations from 1998 to 2021, the trend of the interstitial pressure, the subsidence values measured during the surveys.

2.2   Intervention to mitigate the consolidation processes

Following the damages on buildings due to the consolidation process of the clay layer, the Pioraco Municipality decided in 2009 to realise a pumping well (Figure 4) to feed the aquifer by delivering water from an intake structure close to the artificial channel parallel to the Potenza River. The water pumping operation of was meant to increase the piezometric level

and mitigate the phenomenon of subsidence. Anyway, the injection well activity lasts until February 2018 when it was interested by instability issues.

Figure 4. a) Instability phenomena in correspondence of the pumping well; b) pumping well (modified from Lenci, 2021).

As shown in Figure 5 and Figure 6, the monitoring campaign revealed 1 cm/year of average subsidence for the period 1998-2009 (1.5 cm/year in the central part of the district where the thickness of the clay layer is larger) (Lenci, 2021).

The groundwater pumping test caused increase of the piezometric levels, especially close to the injection point, and the lowering of subsidence rate of buildings to 0.5 cm/year for the period 2009-2012 (Lenci, 2021).

In 2016, the seismic events of August and October caused a groundwater level drop in the entire Umbria-Marche Apennines. The measures revealed an increasing trend for buildings settlement rate (Lenci, 2021).
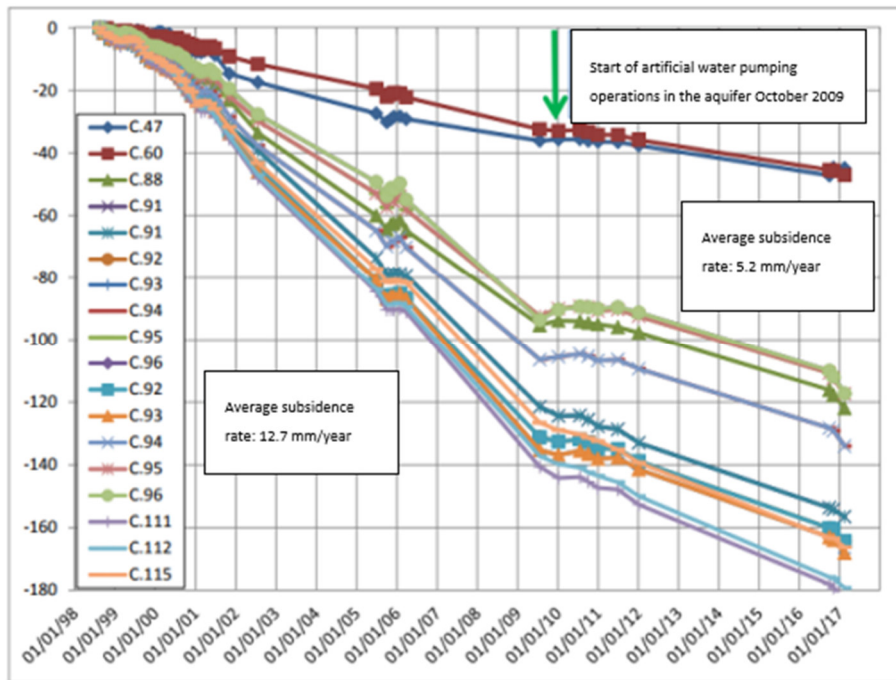
Figure 5. Trend of settlements recorded for each target in the central part of the Madonnetta district (modified from Lenci, 2021).
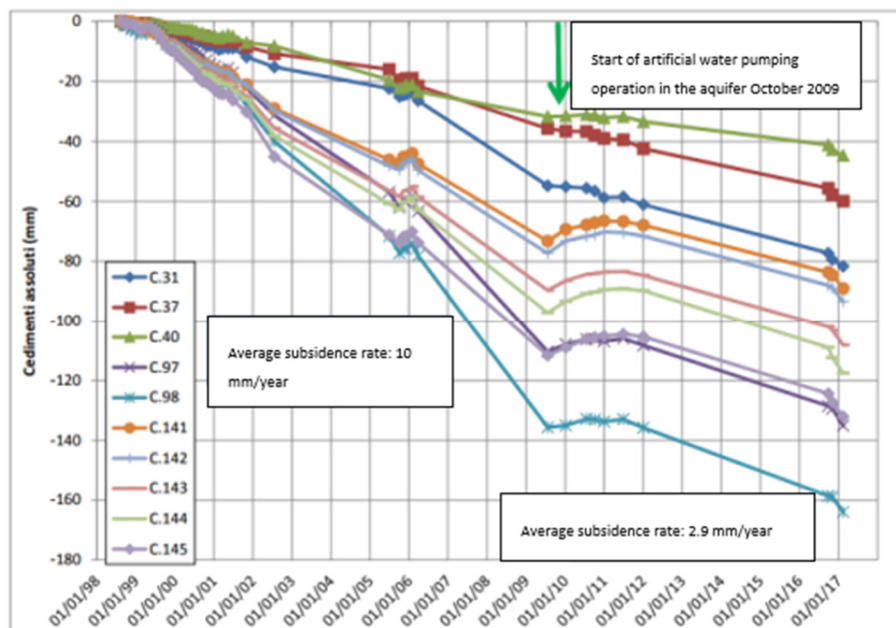

Figure 6. Trend of settlements recorded for each target close to the injection point (modified from Lenci, 2021).

The Madonnetta district is equipped of several piezometers set up into the gravel layer that constitutes, together with the carbonate substrate, the main aquifer (Figure 7).
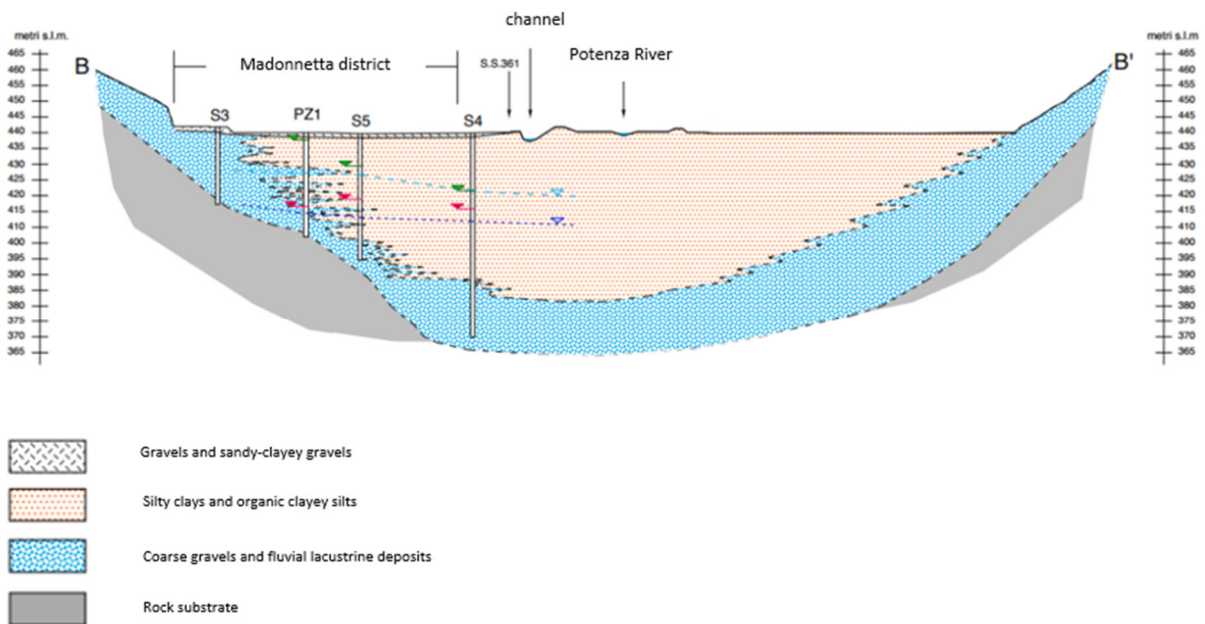
Figure 7. Stratigraphic sections crossing the Madonnetta district, NS direction (modified from Lenci, 2021).

Lenci et al. (2021) started a new geotechnical field campaign to estimate the severity of future failure mechanisms and to evaluate possible operations of reconstruction. To achieve these results it was necessary to assess the characteristics of the clayey deposits from a mechanical and hydraulic point of view and to determine the piezometric levels in the study area. The measures in Table 1 show a variation of groundwater levels around 3 m, increasing in direction of piezometers S4-S5 and reducing both in S16 and S10. Levels variation between February 2012-March 2021 falls within the range of 1 meter (Lenci, 2021).

Denominazione	Profondità dal p.c. (m)	Tipo piezometro	Profondità dell'acqua da p.c. (m)		
			gen-20	feb-21	mar-21
S2	7.4	TA	6,2	5,4	5,4
S4	60	TA	25,0	22,8	22,0
S5	40	TA	20,9	20,6	19,6
S6	12.5	TA	no acqua	no acqua	no acqua
S8	23	TA	no acqua	20,0	-
S10	30	TA	10,7	11,9	11,7
S16	18 *	TA	9,4	13,0	12,0
S18	43 *	TA	11,7	12,0	-
S3(21)	30	CA	-	-	12,5
S8(21)	13.6	CA	-	-	12,5
Pozzo PZ1	33		-	15,8	-
Pozzo privato (PP)	23		-	11,0	-

Table 1. Result of piezometric levelling of 2021 (Lenci, 2021).

On the base of the piezometric levels it was possible to create the isopleths map of the study area referred to the height 440 m a.s.l. and shown in Figure 8.
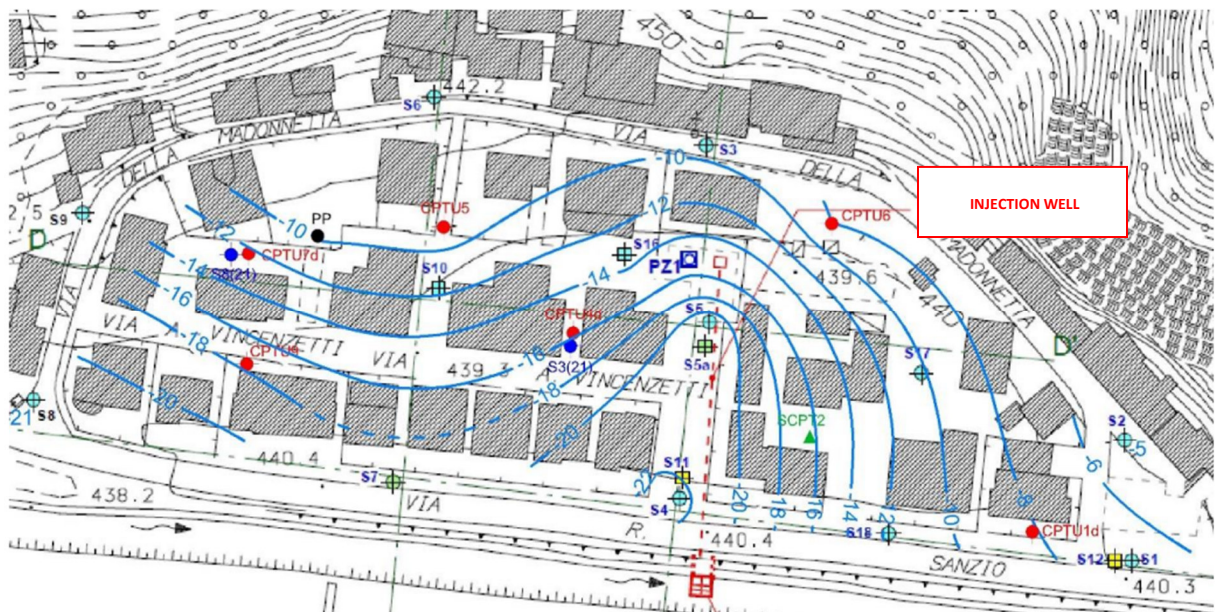

Figure 8. Isopleths reconstruction over the reference height of 440 m a.s.l., February 2021 (modified from Lenci, 2021).

The map shows particularly elevated hydraulic gradients in the district, in particular to the East area close to the injection well (red square). In the central area, the isopleths move towards the direction of piezometers PZ1-S4-S5 located in correspondence of a known direct fault crossing the substratum (Lenci, 2021).

2.3   Seismic microzonation studies in the area

As shown in Figure 9, the Pioraco area has been classified between zones 918 and 919 as result of the seismogenetic zonation ZS9 carried out in 2003 by research group for the assessment of seismic hazard (OPCM n.3274 of 20.03.2003 – INGV – C. Meletti and G. Valensise, 2004). The zone 918 is subjected to NW-vergence compressive tectonic and SE-vergence extensional tectonic that result in earthquakes of magnitude higher than 4.2 (Meletti et al., 2004). The effective depth of the seismogenetic layer is 13 km, that falls within the range 12-20 km and is relatively deeper than other external zones where the seismic events have caused more severe effects (Meletti et al., 2004). Zone 919 is smaller than 918 but characterized by frequent earthquakes of magnitude higher than 5 resulting from the set of direct faults and pronounced by an effective depth of 8 km (Meletti et al., 2004). Figure 10 shows the maximum ground acceleration for Pioraco, 0.175-0.225 ag/g with 10% probability of exceedance in 50 years (Meletti et al., 2004).
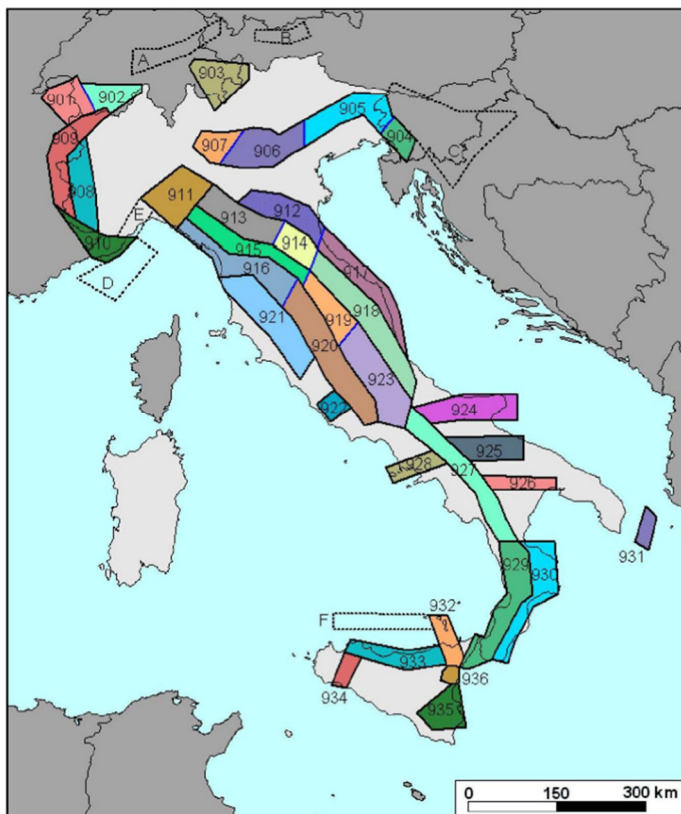

Figure 9. Zone classification provided through the Seismogenetic zonation ZS9 (modified from Meletti et al., 2004).
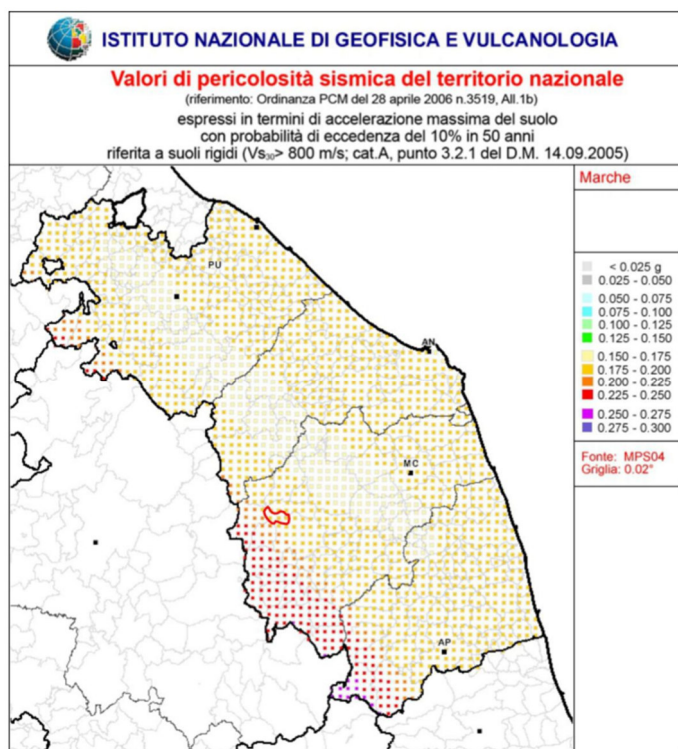
Figure 10. Seismic hazard map of Marche Region from INGV; boundary of Pioraco Municipality in red (modified from Meletti et al., 2004).

In 2015 the territory of Pioraco has been involved in a first level seismic microzonation (SM1) with the purpose of individuating homogeneous microzones and assessing quantitatively the seismic hazard of the area. After the seismic events that strucked the centre Italy in 2016, a third level seismic microzonation (SM3) was performed with the main purpose of rebuilding the geological model of the underground to identify the main substrates and the zones that may potentially be threatened by instability and deformation in case of earthquakes. A third level seismic microzonation requires specific analysis to:

1. Assess the phenomena of seismic resonance potentially representative of amplification phenomena of seismic motion;
2. Determine the S wave velocity profile inside each homogeneous microzone by defining the velocity of each geological formation.

This behaviour follows the phenomenon of Local Seismic Response, which states that waves experience changes in amplitude, frequency and duration when crossing layers of different lithology; this effect is clearly visible between bedrocks and deposits where the wave velocity drops and the wave amplitude increases. In particular, the seismic resonance effects

have been assessed through the Horizontal-to-Vertical Spectral Ratio (HVSR) methodology, a passive seismic technique that uses the environmental noise present everywhere in nature. It is called a passive method because vibrations are not excited ad hoc, such as in other active seismic methods. Ambient-noise vibrations are recorded in the three spatial components and the processing consists of estimating the ratio between the Fourier amplitude spectra of the horizontal (H) to vertical (V) components. The results that can be obtained from HVSR surveys are:

1. the resonance frequency characteristic of the site (main parameter for a correct dimensioning of buildings in order to avoid resonance effect);
2. the fundamental resonance frequency of a building (if measurement is performed inside it) or an estimate of the shear wave velocity Vs (if there is additional information on subsurface geological conditions).

In particular, the seismic microzonation permitted to identify four geological-technical units for substrates and six covering layers (Table 2 and Table 3) and measure the specific velocity of S waves through each unit (Paggi et al., 2017).

	1. Sigla_GEOL	2.Nome formazione	3. Descrizione	4. Tipo_gt
TERRENI I COPERTURA	MUS f1	Depositi travertinosi	sabbie carbonatiche	SMcc
	MUS a	Detriti di versante	ghiaie sabbise e blocchi	GW fd
	MUS e2	Depositi lacustri	argille e limi organici	OH lc
	MUS bn	Depositi di conoide alluvionale	ghiaie sabbise	GC ca
	MUS b2	Depositi eluvioo-colluviali	limi argillosi e sabbiosi	ML ec
	AC bn	Alluvioni Pleistocene medio-sommitale	ghiaie sabbiose	GC tf
SUBSTRATO	FCIe	Formazione di Camerino: litofacis pelitico arenacea	prevalenti strati pelitici alternati a subordinati strati arenacei	COS
	SCH	Formazione dello Schlier	marne, marne siltose calcaree e argillose	ALS
	COI	Formazione della Corniola	calcari micritici	LPS
	MAS	Formazione del Calcare massiccio	calcari a strati spessi e molto spessi	LPS

Table 2. Geological-technical units identified through SM3 (modified from Paggi et al., 2017).

Rock Substratum:

1.   LPS: stratified bedrock that includes the Calcare Massiccio geological formation (MAS) and the Corniola geological formation (COI). Both lithotypes are made of block of rock separated by discontinuities.

2.   ALS: alternance of stratified lithotypes typical of the Schlier formation, a highly fractured rock.

3.   COS: Camerino geological formation, a complex heterogeneous rock: discontinuities are due to the genetic process where different layers have been combined (sandstone-marlstone).

Deposits:

1.   ML ec: colluvial deposits of silt, sandy silt and clayey silt.

2.   OH lc MUSe2: lacustrial deposits made of organic silt and organic clay, located around Pioraco and along Scarzito River.

3.   SMcc: sand and carbonate silty sand.

4.   GW fd: gravels of different granulometry such as slope debris.

5.   GC ca: sandy gravels.

6.   GC tf: alluvial sandy gravels.

GT	Description	LOG	Vs med (m/s)	Vs Min (m/s)	Vs max (m/s)
LPS	MAS	SS	1150	899	1388

GT	Description	LOG	Vs med (m/s)	Vs Min (m/s)	Vs max (m/s)
ALS	SCH	SG	510	501	523
ALS	SCH	SS	850	810	910

GT	Description	LOG	Vs med (m/s)	Vs Min (m/s)	Vs max (m/s)
COS	FCle	SG	600	354	721

GT	Description	LOG	Vs med (m/s)	Vs Min (m/s)	Vs max (m/s)
ML ec	MUSb2	TC	180	134	223

GT	Description	LOG	Vs med (m/s)	Vs Min (m/s)	Vs max (m/s)
OH lc	MUSe2	TC	170	106	243

GT	Description	LOG	Vs med (m/s)	Vs Min (m/s)	Vs max (m/s)
OH lc	MUSe2	TC	250	207	320

GT	Description	LOG	Vs med (m/s)	Vs Min (m/s)	Vs max (m/s)
GW fd	MUSa	TC	600	223	967

GT	Description	LOG	Vs med (m/s)	Vs Min (m/s)	Vs max (m/s)
GC ca	MUSbn	TC	350	298	479

GT	Description	LOG	Vs med (m/s)	Vs Min (m/s)	Vs max (m/s)
GC tf	AC bn	TC	640	516	777

Table 3. Geological-technical units identified through SM3 (modified from Paggi et al., 2017).

Five geological sections (Figure 11, Figure 12, Figure 13, Figure 14, Figure 15) have been produced to build the geological-technical map (CGT) and identify the homogeneous microzones of seismic prospective (MOPS). The geological sections highlight the interface between substrate and cover layers as main responsible of the amplification of seismic motion (Paggi et al., 2017). The rock substrate was characterized through geostructural measurements focusing on lithology and fracturing degree. The rock substratum falls in stable areas with amplifications due to the steepness of topographic surface larger than 15° (Paggi et al., 2017). The covering layers may be classified into:

1. Fluvial-lacustrine deposits, both in Potenza River and Scarzito River, made of an underlying layer of gravel where a silt deposit layer stands; these two different units have different seismic characteristics and thickness, ranging from 6 to 75 meters;

2. Travertine deposit lying below the Pioraco centre, covering a 75.000 m^2 area with a thickness around 70 meters;

3. Slope deposits along the Scarzito valley, consisting of debris flow accumulation or rockfalls and marginally into conjunction zone between rocky walls and valley floor (Paggi et al., 2017).

About these layers, a representative minimum and maximum thickness has been hypothesized by performing geological sections, analysing geological surveys and comparing with the results of HVSR measures.
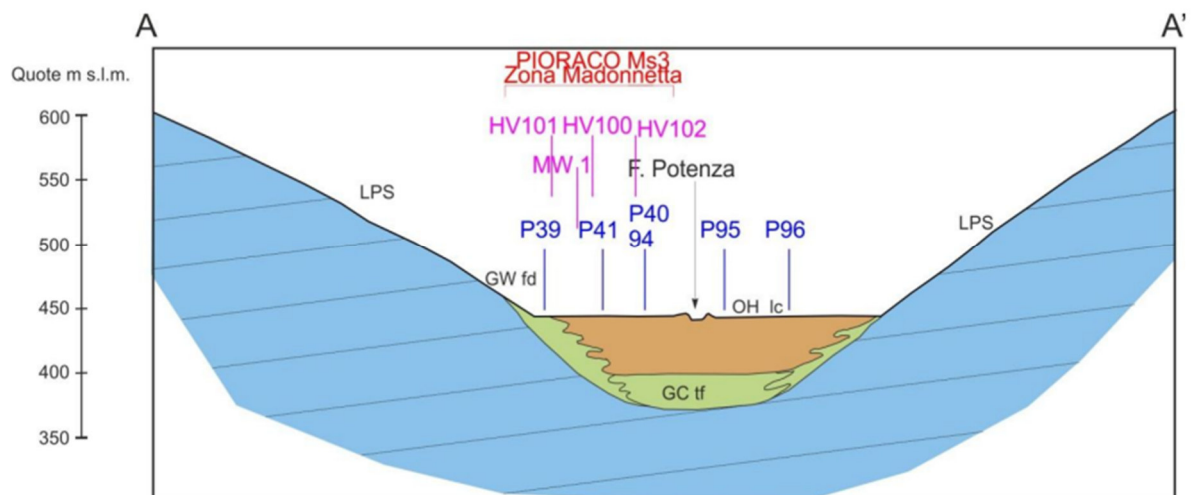
Figure 11. Geological section passing through the Potenza River valley across the fluvial-lacustrine deposits (modified from Paggi et al., 2017).
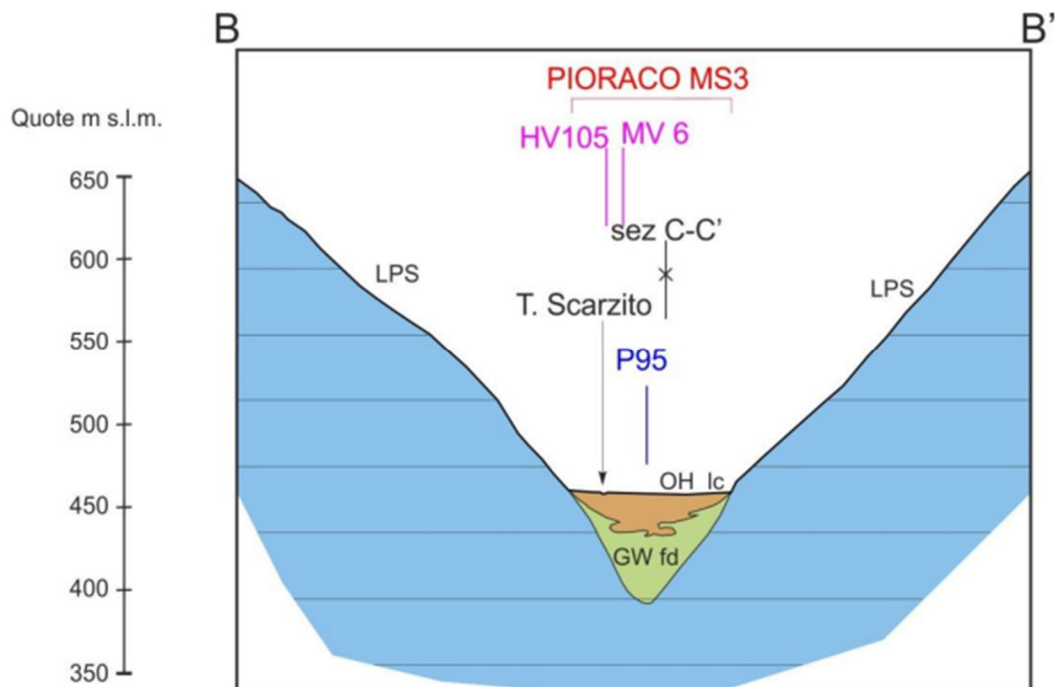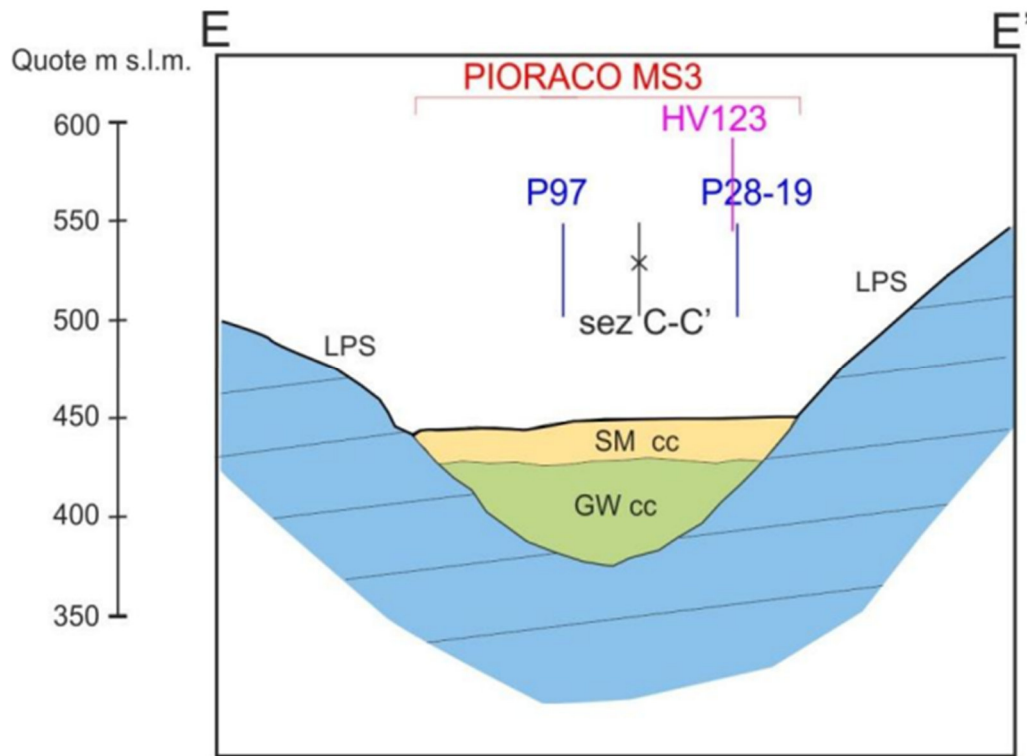
Figure 12. Geological section passing through the Pioraco city centre across the travertine (modified from Paggi et al., 2017).

Figure 13. Geological section along Scarzito River through fluvial-lacustrine deposits (modified from Paggi et al., 2017).
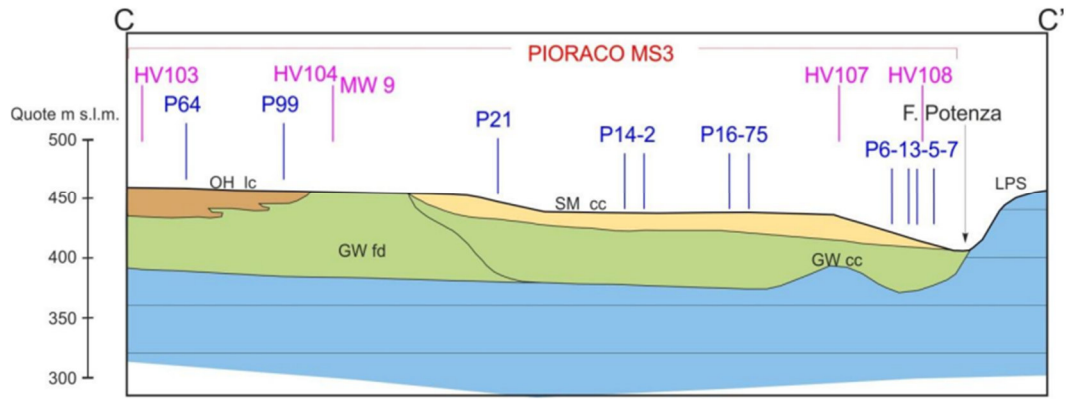
16

Figure 14. Geological section of Scarzito valley and Potenza valley junction (modified from Paggi et al., 2017).
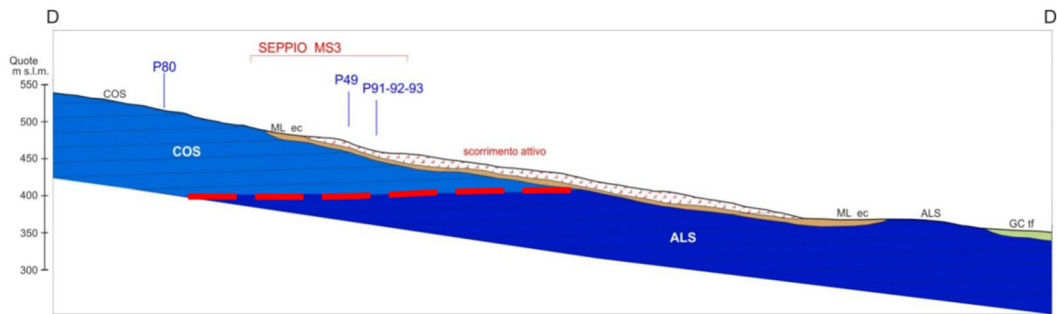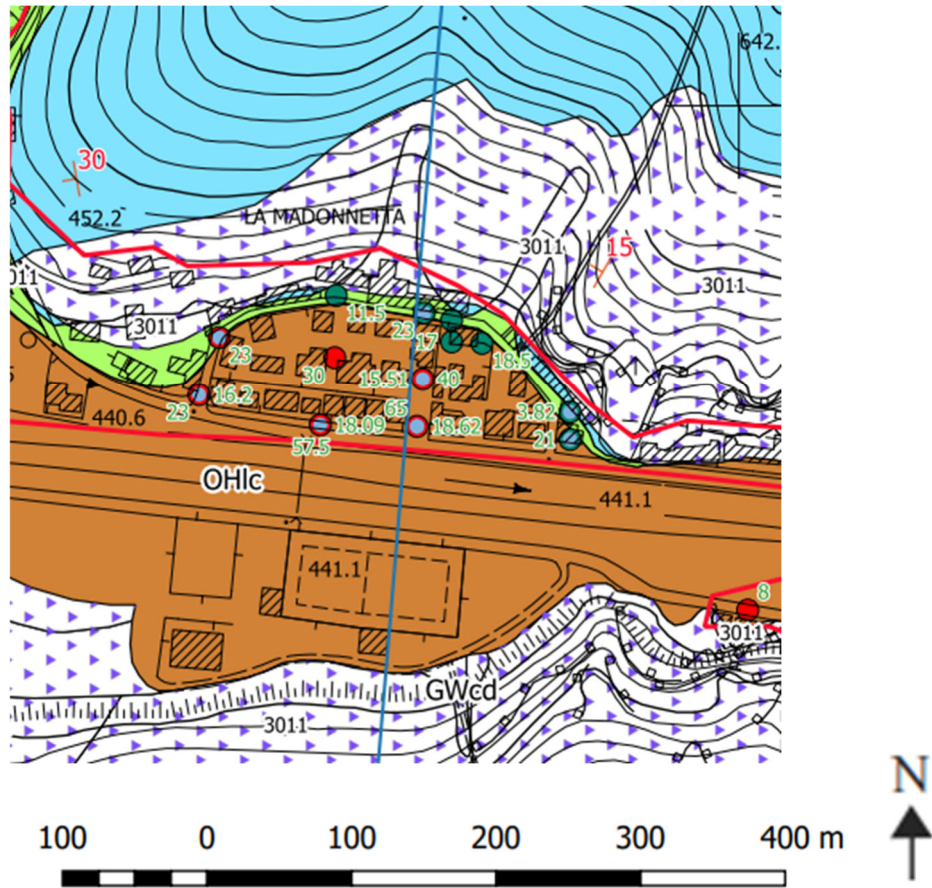

Figure 15. Geological section through Seppio town (modified from Paggi et al., 2017).

Figure 16 displays the Geological Technical Map realised after the Seismic Macrozonation Level 3 (Paggi et al., 2017).
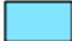

Figure 16. Map detail of the Madonnetta district in Pioraco town, from geological-technical map (CGT), scale 1:5000 (modified from Paggi et al., 2017).

Table 3 reports the classification of the identified homogeneous microzones of seismic prospective (MOPS), based on minimum and maximum thickness of each geological unit,

depth of seismic substrate, geologic substrate, seismic substrate, S waves mean, maximum and minimum velocity.

COMUNE	MOPS	SPESSORE MIN (m)	SPESSORE MAX (m)	PROFONDITA' BEDROCK MIN (m)	PROFONDITA' BEDROCK MAX (m)	TIPO_GT	SIGLA GEOL o Descrizione	LOG	Vs med (m/s)	Vs Min (m/s)	Vs max (m/s)
PIORACO	2001	40	80			COS	FCIe	SG	550	403	620
				40	80	ALS	SCH	SS	850	810	910
	2002	1	15			ALS	SCH	SG	510	501	523
				1	15	ALS	SCH	SS	850	810	910
	2003	5	20			SM cc	MUSf1	TC	250	182	344
		1	50			GW cc	MUSf1	TC	400	245	589
				6	70	LPS	MAS	SS	1150	899	1388
	2004	5	70			GW fd	MUSa	TC	600	223	967
				5	70	LPS	MAS, COI	SS	1150	899	1388
	2005	40	50			OH lc	MUSe2	TC	170	106	243
		10	30			GC tf	MUSa	TC	320	289	357
				60	70	LPS	MAS, COI	SS	1150	899	1388
	2006	5	25			OH lc	MUSe2	TC	250	207	320
		1	45			GW fd	MUSa	TC	600	556	647
				6	75	LPS	MAS, COI	SS	1150	899	1388
	2009	10	30			GC ca	MUSbn	TC	350	298	479
				10	30	LPS	COI	SS	1150	899	1388
	2010	10	20			ML ec	MUSb2	TC	180	134	223
		1	15			ALS	SCH	SG	510	501	523
				11	25	ALS	SCH	SS	850	810	910
	2011	3	15			GC tf	AC bn	TC	640	516	777
				3	15	ALS	SCH	SS	850	810	910
	2012	3	10			ML ec	MUSb2	TC	200	197	217
		40	80			COS	FCIe	SG	550	403	620
				45	85	ALS	SCH	SS	850	810	910
	2013	5	45			OH lc	MUSe2	TC	170	106	243
		1	25			GC tf	MUSa	TC	320	289	357
				6	60	LPS	MAS, COI	SS	1150	899	1388
	2014					LPS	MAS, COI	SS	1150	899	1388

Table 4. Homogeneous microzones of seismic prospective (MOPS) identified through SM3 (modified from Paggi et al., 2017).

In Figure 17 the stratigraphic columns representative of the identified microzones are presented while Figure 18 shows the Map of Macrozones of Seismic Prospective. One can notice that the area of the Madonnetta district is classified as zone of differential settlements (Paggi et al., 2017).
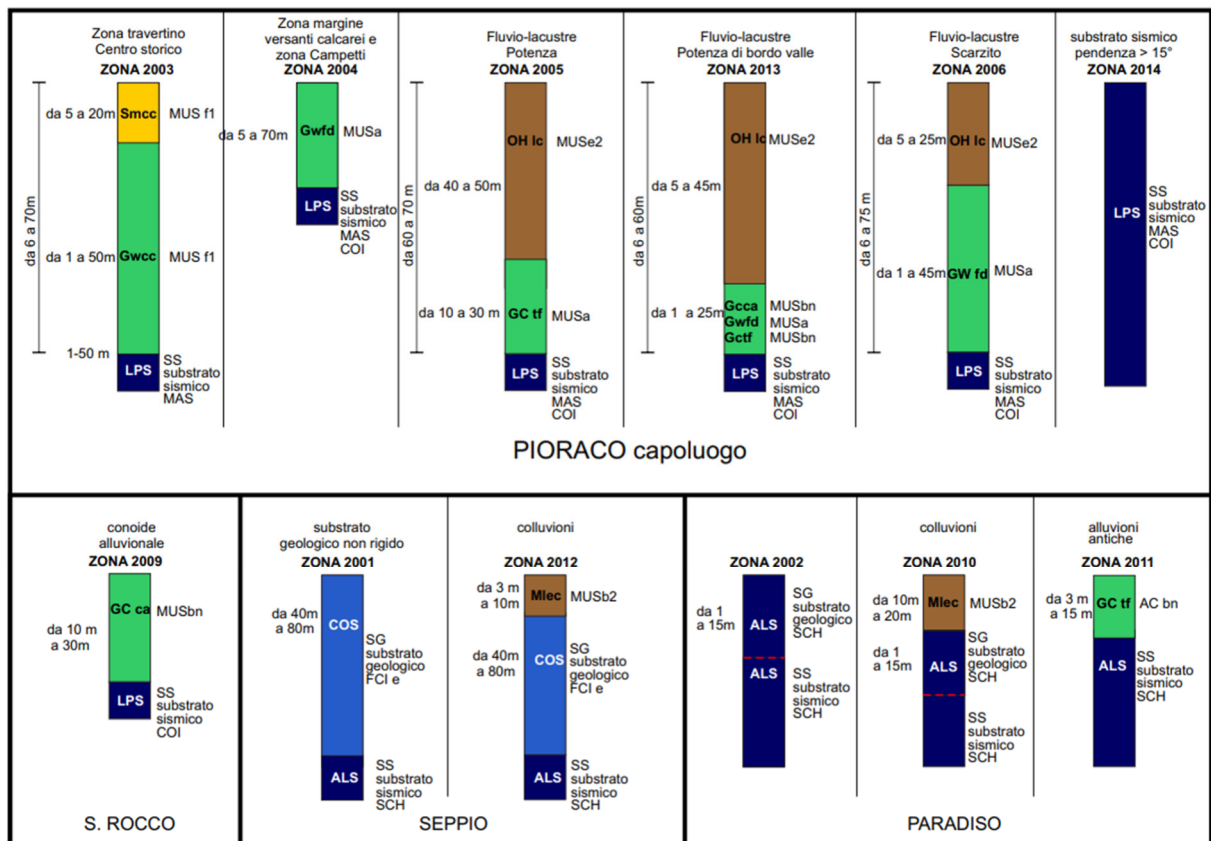
Figure 17. Stratigraphic columns representative of microzones (modified from Paggi et al., 2017).
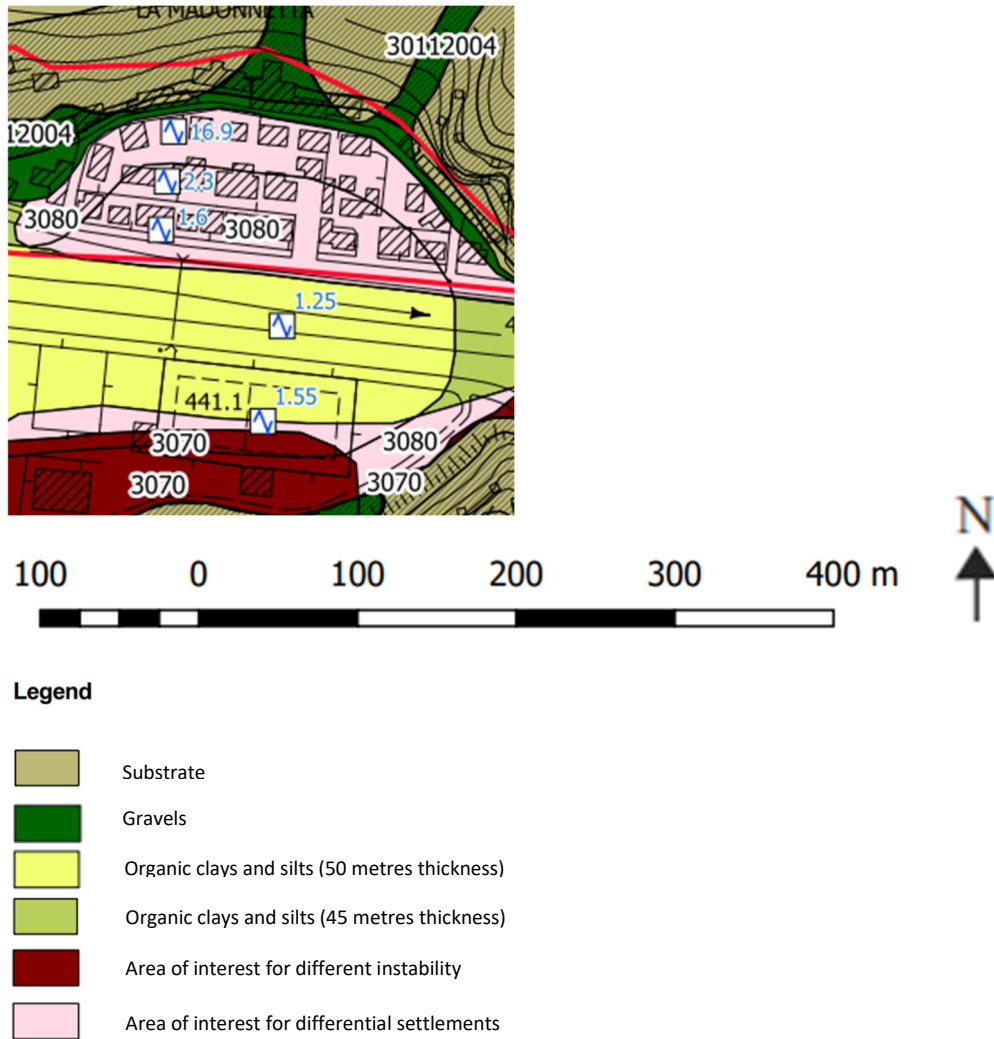
Figure 18. Map of homogeneous microzones of seismic prospective (MOPS), scale 1:5000 (modified from Paggi et al., 2017).

2.4 Subsidence monitoring: topographic levelling and DInSAR analysis comparison

This area had been under observation through ground-based monitoring surveys since 1998 (following the previous seismic event in 1997) until 2021. The DInSAR (Differential Interferometric Synthetic Aperture Radar) analysis was carried out exploiting Sentinel-1A/B data during the period 2014-2021. The goal of the DInSAR processing stage of the procedure is to derive the deformation map of the area of interest from SAR data. A "zero date" has been set for both survey methods in order to define similar time series for comparison analysis (Di Stefano et al., 2022).

The first levelling campaign was carried out in 1998. It was necessary for an initial data collection to monitor the area following the earthquake in the central Apennines (Marche-Umbria Regions) in 1997. A total of 49 levelling surveys have been carried out since then, the last one dating back to January 2021 (Table 4). As can be seen from the list of surveys carried out, in the first 4 years (between 1998 and 2001) monitoring operations were constant with a total of 31 surveys. From 2002 onwards, surveys were carried out occasionally and mainly following the major seismic events that hit the regions of Central Italy in 2009 and 2016-2017. The monitoring campaigns were carried out with topographic levelling by using the targets, in the form of metal bolts, attached in the corners of building facades. Two fixed markers (indicated with n. 1 and n. 23 in yellow in Figure 19 attached on the closer rock face, are the reference system to monitor the variations of other 172 targets (Di Stefano et al., 2022).

No. survey	Date	No. survey	Date	No. survey	Date
1st and 2nd	17-18/08/1998	18th	07/04/2000	34th	03/10/2005
3rd	21/09/1998	19th	10/05/2000	35th	09/11/2005
4th	19/10/1998	20th	12/06/2000	36th	06/12/2005
5th	27/11/1998	21st	18/07/2000	37th	30/01/2006
6th	04/01/1999	22nd	18/08/2000	38th	27/03/2006
7th	21/02/1999	23rd	18/09/2000	39th	21/07/2009
8th	02/04/1999	24th	23/10/2000	40th	07/01/2010
9th	17/05/1999	25th	26/11/2000	41st	20/07/2010
10th	20/06/1999	26th	10/01/2001	42nd	04/10/2010
11th	27/07/1999	27th	19/02/2001	43rd	30/12/2010
12th	01/09/1999	28th	26/03/2001	44th	29/06/2011
13th	17/10/1999	29th	15/05/2001	45th	04/01/2012
14th	26/11/1999	30th	29/06/2001	46th	28/09/2016
15th	28/12/1999	31st	03/11/2001	47th	05/11/2016
16th	01/02/2000	32nd	22/07/2002	48th	13/02/2017
17th	28/02/2000	33rd	29/06/2005	49th	29/01/2021

Table 5. List of topographic levelling network surveying (from Di Stefano et al., 2022).

Figure 19. Targets of the topographic levelling network with identification of the two fixed markers (in yellow) (modified from Di Stefano et al., 2022).

In order to compare and complement the topographic levelling data, a DInSAR analysis was carried out with SAR images acquired by the Sentinel-1 polar-orbiting satellites of ESA (https://sentinel.esa.int/web/sentinel/missions/sentinel-1). The processing of these SAR images makes it possible to estimate the velocity map and the time series of deformation of some points detected in an area of interest (Di Stefano et al., 2022). A total of 324 Single Look Complex Sentinel-1 images were collected with a minimum revisit period of 6 days.

For what concerns the coordinates of levelling points, they are georeferenced on WGS84-UTM zone 33N (EPSG 25833). The targets were mapped in the QGIS software. The ground subsidence was elaborated basing to the time series of levelling monitoring, shown in Figure 20, relating to the most significant periods connected to the recent seismic events (2016-2017) that have affected the area of interest. The values reported in the legends, referring to the intervals (5 ranges are displayed) of vertical displacements, are expressed in millimetres.

Figure 20. a) Ground displacements, expressed in millimetres, measured through the topographic levelling for period 04/10/2012-28/09/2016; b) Ground displacements, expressed in millimetres, measured through the topographic levelling for period 28/09/2016-05/11/20 (modified from Di Stefano et al., 2022).

The output of the DInSAR processing is a deformation map composed of a set of selected geocoded points, called Persistent Scatterers (PSs), with information on the estimated LOS

(line of sight) velocity of deformation (Figure 21) and the accumulated deformation at each Sentinel-1 image acquisition time (Di Stefano et al., 2022). Interferometer based techniques delivers deformation maps of soil measured along the line of sight of the sensor; furthermore, one is allowed to follow the evolution of the deformation itself on the base of a set of images previously captured (Di Stefano et al., 2022).

Figure 21. Deformation velocity map (processing period 2014- 2021) with the corresponding legend with 5 ranges of terrain displacement values expressed in millimetres (modified from Di Stefano et al., 2022).

As stated above, topographic levelling surveys started in 1998. To compare the data with those point measurements identified with DInSAR and, considering that the Sentinel-1A mission started in 2014, it has been decided to consider the data acquired in the same temporal period. Therefore, the topographic levelling carried out in 2012 (survey no. 45) is considered as the new "zero date" for subsidence analysis (Figure 22).
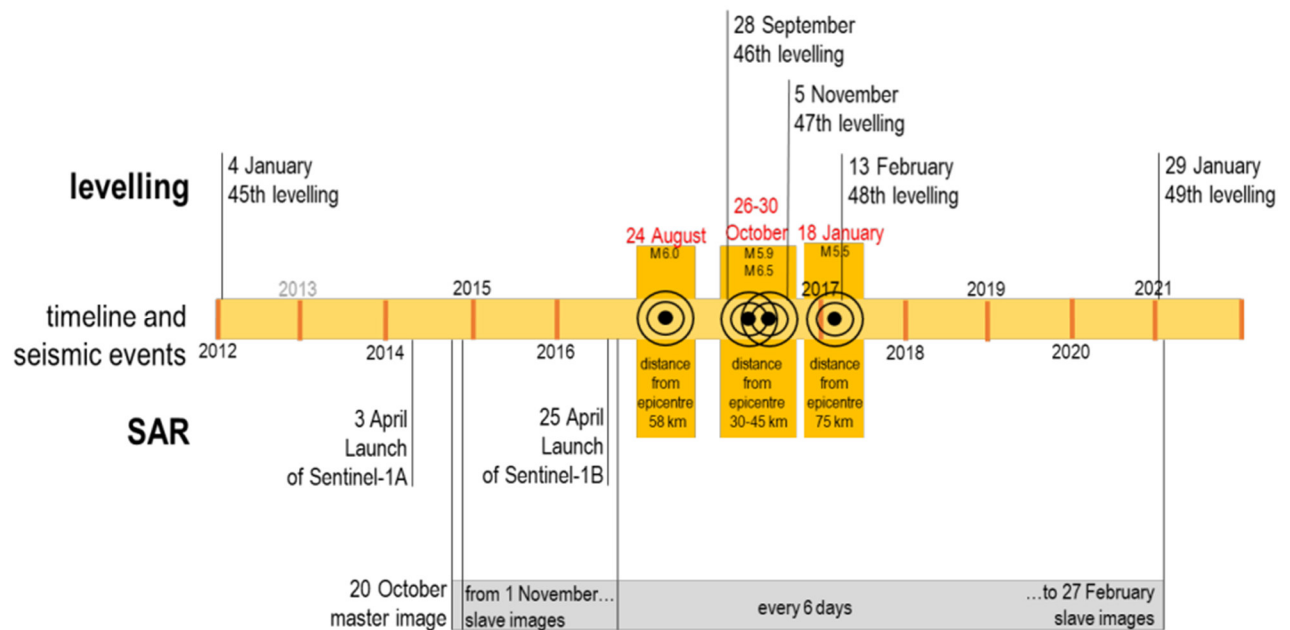
Figure 22. Chronologic line of topographic levelling and InSAR analysis (modified from Di Stefano et al., 2022).

It should be remembered that one compares two systems that give results on different components of ground subsidence: the data obtained from topographic levelling concern only the scalar vertical displacement; the subsidence recorded by SAR data is measured in LOS (line of sight). In determining the ground subsidence rate based on SAR points, "stable points" encoded by the SAR images were identified, indicated in green in Figure 23. A check was made for the presence of SAR points (range of values close to zero) near the fixed points of the topographic levelling. Close to the topographic levelling reference point no. 23, there are no SAR points; on the other hand, regarding the topographic levelling reference point no. 1, several SAR points are present at a short distance on the rock relief.

Figure 23. Map of "stable points", in white from topographic levelling (reference points are indicated by the red arrow) and in green from DInSAR (modified from Di Stefano et al., 2022).

To identify the "stable points" among the DInSAR geocoded points, a statistical analysis was carried out based on the calculation of polynomial regression and the analysis of dispersion index with respect to the mean value curve. A graph showing the ground subsidence values of each geocoded point has along the x-axis the number of processed DInSAR images in temporal order and along the y-axis the ground subsidence values over time, in millimetres. The third-degree polynomial curve is drawn, and the squared regression coefficient value (R^2) associated to the trend of this curve is calculated (Figure 24). If the third-degree polynomial curve shows an almost linear trend, parallel to the linear curve, with a value of both regression closer to 0, the point is considered "stable" (Di Stefano et al., 2022).

$$y = 1E\text{-}07x^3 - 7E\text{-}05x^2 + 0,0275x - 0,2838$$
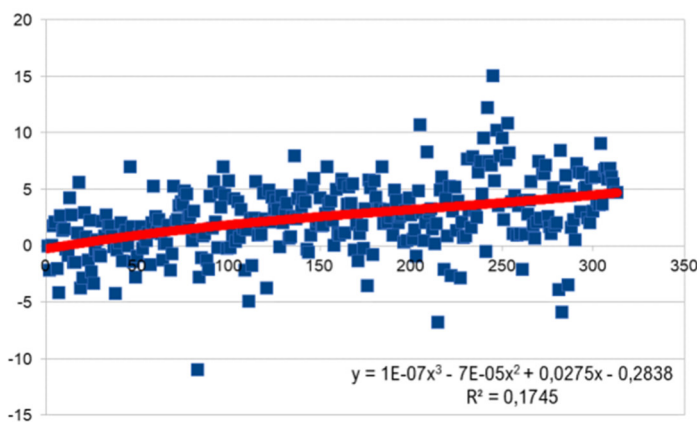$$R^2 = 0,1745$$

Figure 24. Graph of values referring to point no. 438, third degree polynomial curve, equation and its regression (modified from Di Stefano et al., 2022).

The comparison of the analysis, made on QGIS software, showed that ground displacements measured by levelling (Figure 25) and DInSAR (Figure 26) have similar trends in the results. On the geomorphological aspect, the same distribution map of terrain subsidence is found in both techniques (Di Stefano et al., 2022).
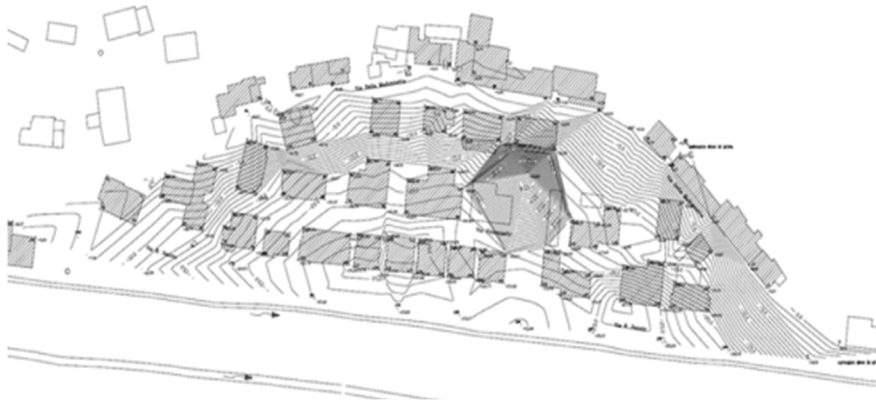

Figure 25. Map of the subsidence curves generated from the analysis of topographic levelling data (modified from Di Stefano et al., 2022).
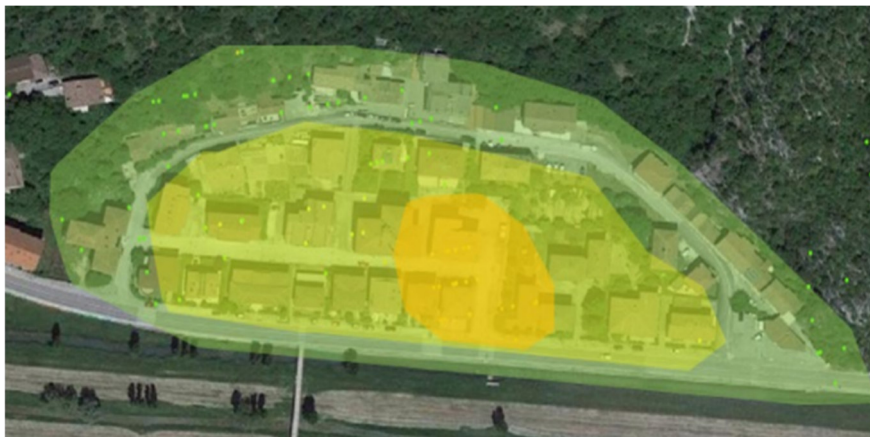

Figure 26. Heat map of the terrain subsidence from the elaboration of DInSAR data (modified from Di Stefano et al., 2022).

In addition, a pointwise analysis was carried out to specifically examine this comparison between topographic levelling and DInSAR. In this phase, several points measured with levelling and located in the proximity of DInSAR ones were compared to make a first assessment. The operation was carried out on 10 points that gave the same feedback. Figure 27 shows one of the points taken to compare the terrain subsidence: n. 99 from topographic levelling and the proximal n. 411 from DInSAR.
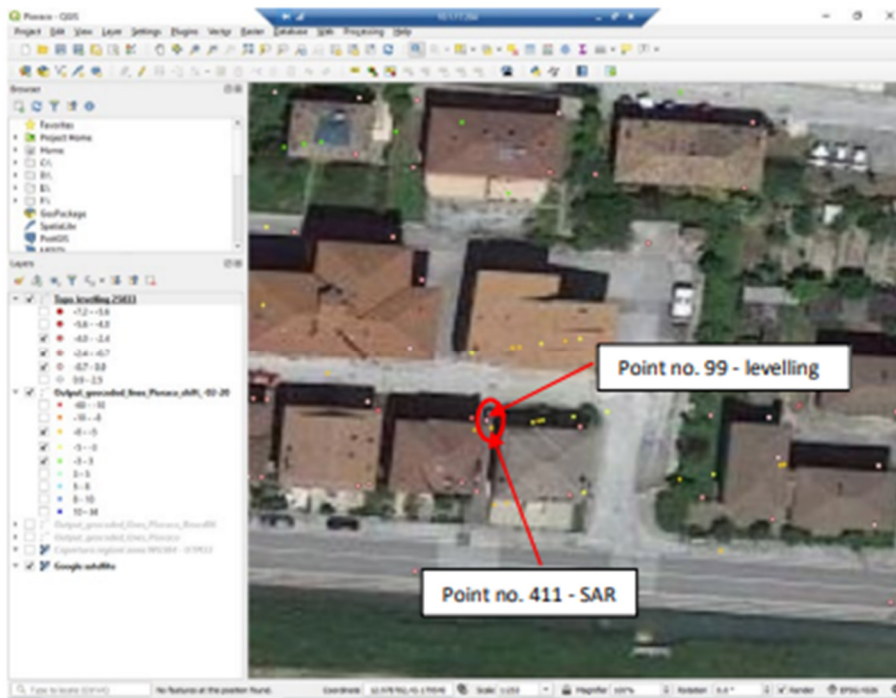
Figure 27. Identification of points for pointwise analysis: no. 99 from topographic levelling and the proximal no. 411 from DInSAR (modified from Di Stefano et al., 2022).

Point n. 99 shows a subsidence of more than 20 mm while point n. 411 has a maximum subsidence value of the order of 10-12 mm (in LOS, almost vertical), which is lower than the value of the proximal levelling point (n. 99). As a first consideration it can be stated that terrain subsidence is highlighted in both results (Di Stefano et al., 2022). The different subsidence value between the two surveys (about 10 mm) suggests that in the time interval 2012-2014, previous to SAR survey, there might have been a subsidence phenomenon not related to seismic events (Di Stefano et al., 2022). Maybe some geological or geo-mechanical phenomenon may have occurred due to the fact there are a fault, a surface water table, and the clay component of the soil. Stable points were defined as those points that did not show a significant variation in subsidence. So-called moving points are those that have registered subsidence values greater than 1 mm. The analysis between stable points have showed same trend in the variation of terrain subsidence between topographic levelling and DInSAR. Similar trend is confirmed also from the comparison between moving points of both survey techniques (Di Stefano et al., 2022).

3. Geological outlines of the Umbria-Marche Apennines

The Umbria-Marche ridge, located in Northern Apennines, is the westernmost of the two main ridges that form the Umbria-Marche Apennines as displayed in Figure 28 (Centamore et al., 1991). The map covers an area about 50 km^2 wide, located in the west sector of the Marche region (Province of Macerata) and falls within the drainage basin of the Potenza river; the main villages in the area are Pioraco and Sefro (Fabbi, 2015).
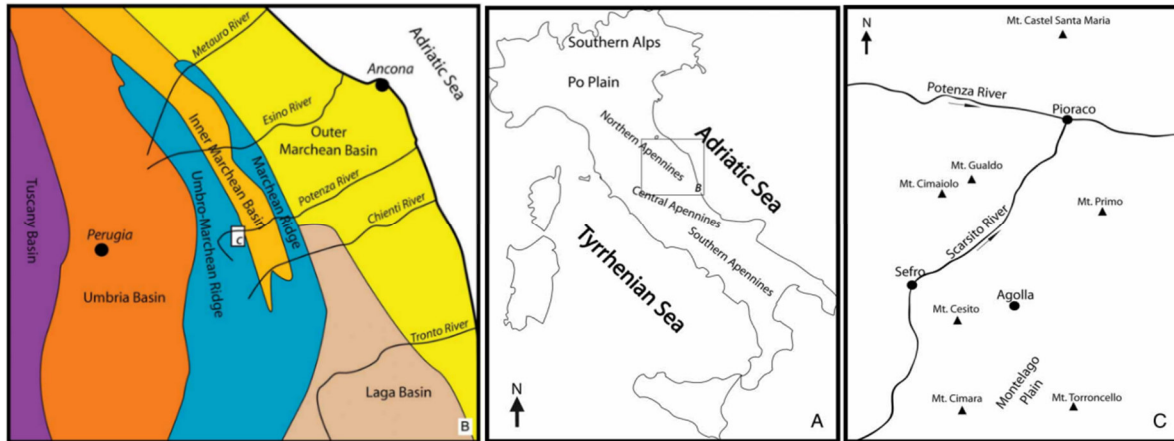

Figure 28. Regional overview and location of the study area (modified from Fabbi, 2015).

The Umbria-Marche Apennines in central Italy is a North-East vergent, arcuate, fold and thrust belt nucleated from Late Miocene to Early Pliocene age (Barchi et al., 1993). The sedimentary sequence (Figure 29) involved in the deformation consists of the following groups of geological formations, from the top to the bottom:

1. Flysch-type turbidites (Tortonian-Messinian age), varying in thickness from 1000 to 3000 m;
2. Cherty limestones and marls (Oligocene to Middle Jurassic), forming a thin-bedded pelagic multi-layer (about 1300 m) (from top to bottom: Scaglia Cinerea Fm., Scaglia Rossa Fm., Marne a Fucoidi Fm., Maiolica Fm., Calcari Diasprini Fm., Rosso Ammonitico Fm., Corniola Fm.);
3. Massive limestones of the carbonate shelf (Early Liassic), with an estimated thickness of about 700 m (Calcare Massiccio Fm);

4. Thinly bedded limestones and marls (upper part of Late Triassic), with a thickness of about 100 m;

5. Evaporites (Late Triassic), comprising mainly dolomites and anhydrites (Anidriti di Burano Fm), with an assumed thickness between 1000 and 2000 m (Barchi et al., 1993).
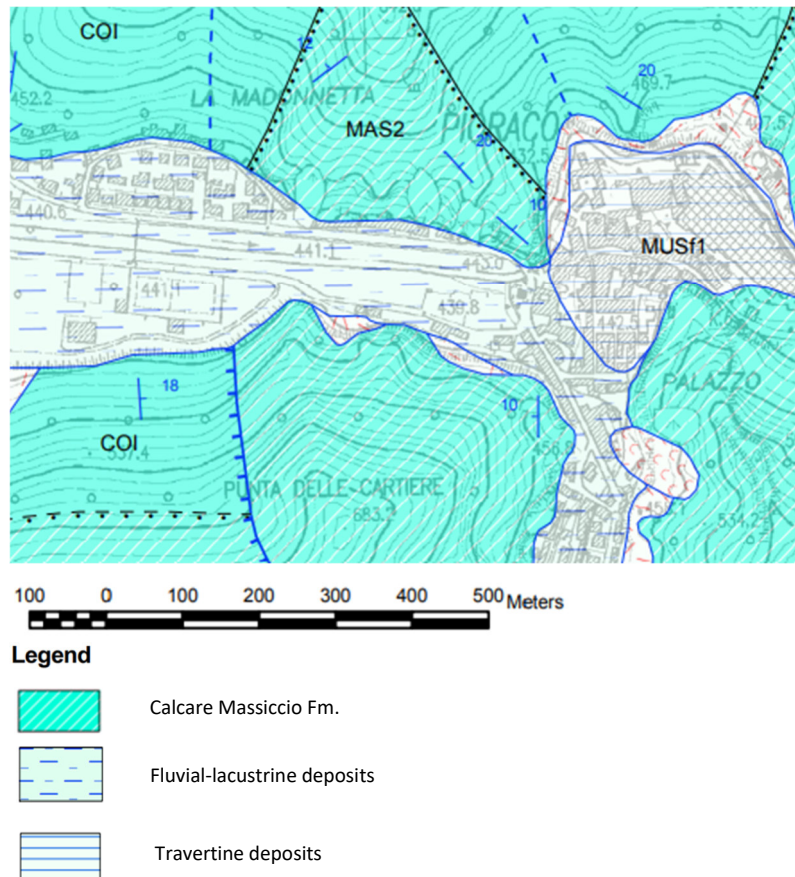

Figure 29. Detail of the geological succession in Madonnetta district and Pioraco centre, (adopted from Marche Region geological map, section 312040, scale 1:10.000).

3.1 Geology of the study area

During Holocene, along the Potenza valley important arrangements occurred which led to the formation of Sefro lake, the Pioraco-Fiuminata lake and the deposition of Pioraco travertine (Paggi et al., 2017). Geophysical investigations revealed the presence of 70-80 meters of debris and fluvial-lacustrine deposits along the valleys of Scarzito River and Potenza River (Figure 30). Before getting filled by sediments, the morphology of the two valleys was tight and deep, with steep and vertical slopes that caused several rockfalls especially after earthquakes (Paggi et al., 2017). Today there is a twenty meters gap between Scarzito River

and Potenza River, but it is possible to say that originally they constituted a continuous hydrodynamic profile (Paggi et al., 2017).
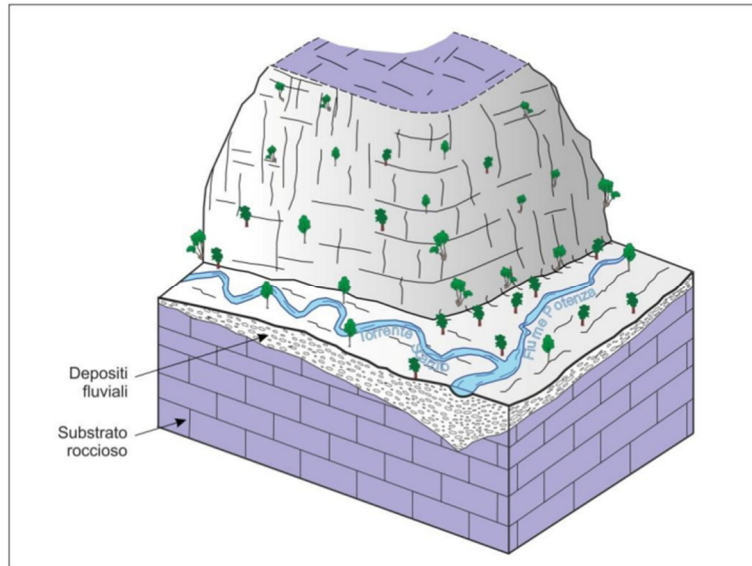

Figure 30. Original configuration of Scarzito and Potenza valleys (modified from Paggi et al., 2017).

This configuration was modified by rockfalls and debris landslides that block the Scarzito valley, occluding the water flow and creating the so called Sefro lake (Figure 31), upstream of Pioraco (Paggi et al., 2017). At the same time, the morphological step that accommodate the deposition of Pioraco travertine was created (Paggi et al., 2017). Later on, the travertine clogged the Potenza River and deviate it to the North, progressively creating a barrier towards the main valley (Figure 32) (Paggi et al., 2017).
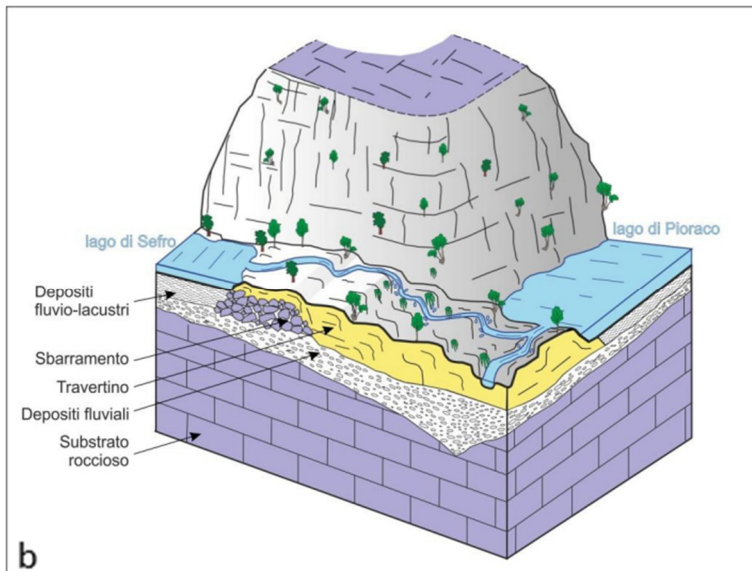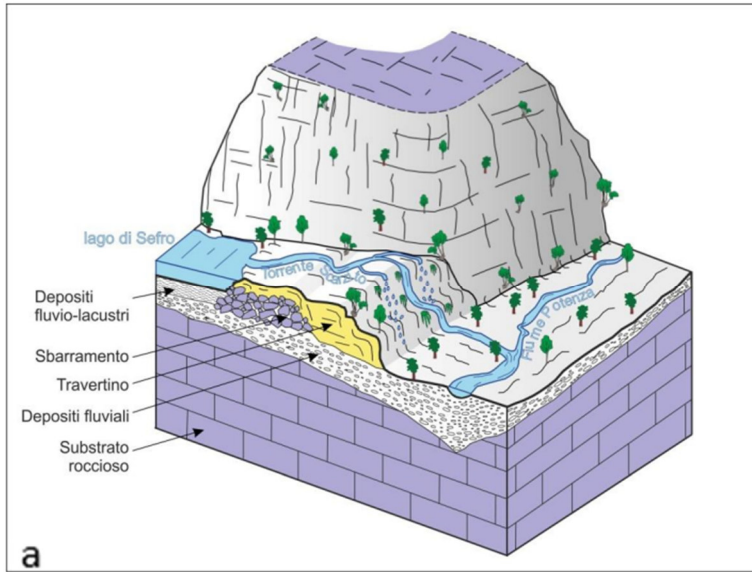
Figure 31. a) Formation of the Sefro Lake and the morphological step; b) formation of the Pioraco Lake due to travertine occlusion of Potenza valley (modified from Paggi et al., 2017).
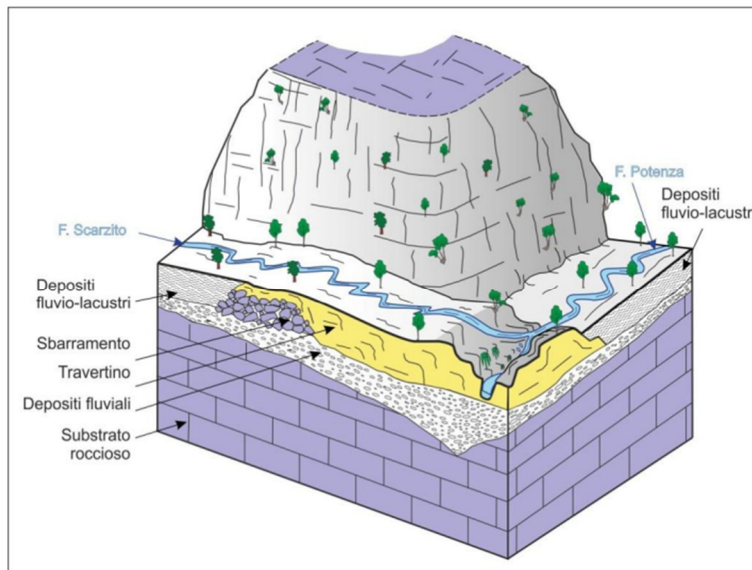
Figure 32. Actual configuration of the area, featured by the morphological step; the former lakes are filled by fluvial lacustrine deposits (modified from Paggi et al., 2017).

A geological map on the 1:15.000 scale is presented in Figure 34, displaying the geology of a portion of the Umbria-Marche ridge in correspondence of Pioraco village (Figure 33) and illustrating the main stratigraphic, paleogeographic and structural features of the area (Fabbi, 2015). The geological formation outcropping in the area are the Calcare Massiccio formation (lower Jurassic), the Corniola formation and the alluvial deposits (Figure 34). The contact between the Calcare Massiccio Fm. and the Corniola Fm. is a tectonic boundary expressed by a normal fault.

Figure 33. Localization of Pioraco (by Google Earth).

ALLUVIAL DEPOSITS
Yellow/grey silt-clays, sands and conglomerates with polygenic rounded lithoclasts.

CORNIOLA FM.
(Sinemurian *p.p.* - Pliensbachian)
Grey-hazel lime mudstone and wackestone with common radiolarians, sponge spicules, brachiopods, ostracods and benthic forams. The lower portion bears great volumes of resedimented benthic material, organized in thick graded and laminated beds. Upper portion is a well bedded pelagic mudstone with white chert nodules.

CALCARE MASSICCIO FM.
(Hettangian - Sinemurian *p.p.*)
White grainstone, massive to faintly bedded, containing bioclasts (gastropods and bivalves), ooids, oncoids, peloids, ostracods, corals, benthic forams, algae (Dasycladaceae, Solenoporaceae). Red levels rich in vadose pisoids and Fe-oxides indicate phases of subaerial exposure.
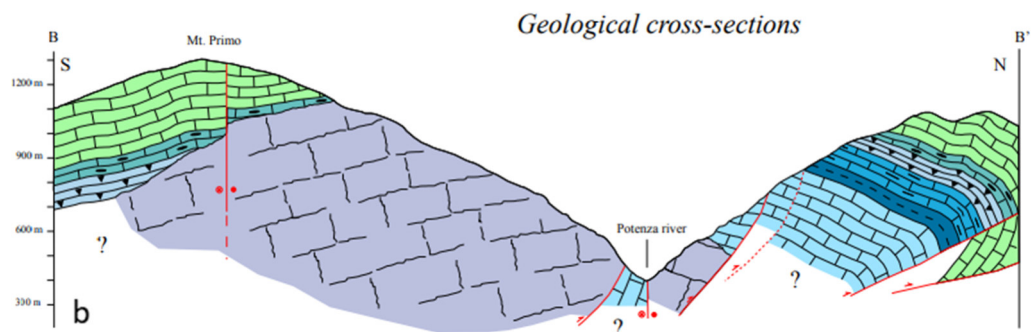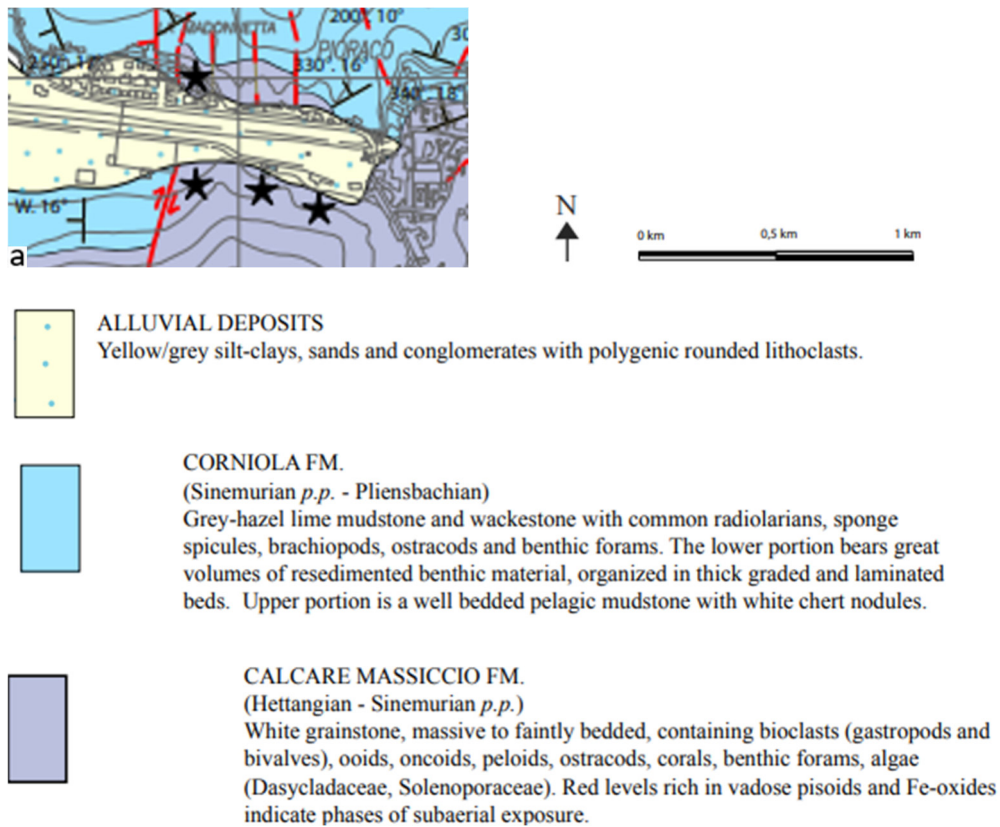

Figure 34. a) Detail of geology and Jurassic paleogeography of the Mt. Primo-Mt. Castel Santa Maria ridge and neighbouring areas (modified from Fabbi, 2015); b) Geological cross-section of the Pioraco area (modified from Fabbi, 2015).

The territory around Pioraco is characterized by Mesozoic-Tertiary calcareous and marly formations that belong to the Umbria-Marche Stratigraphic Succession (Figure 35) (Paggi et al., 2017).
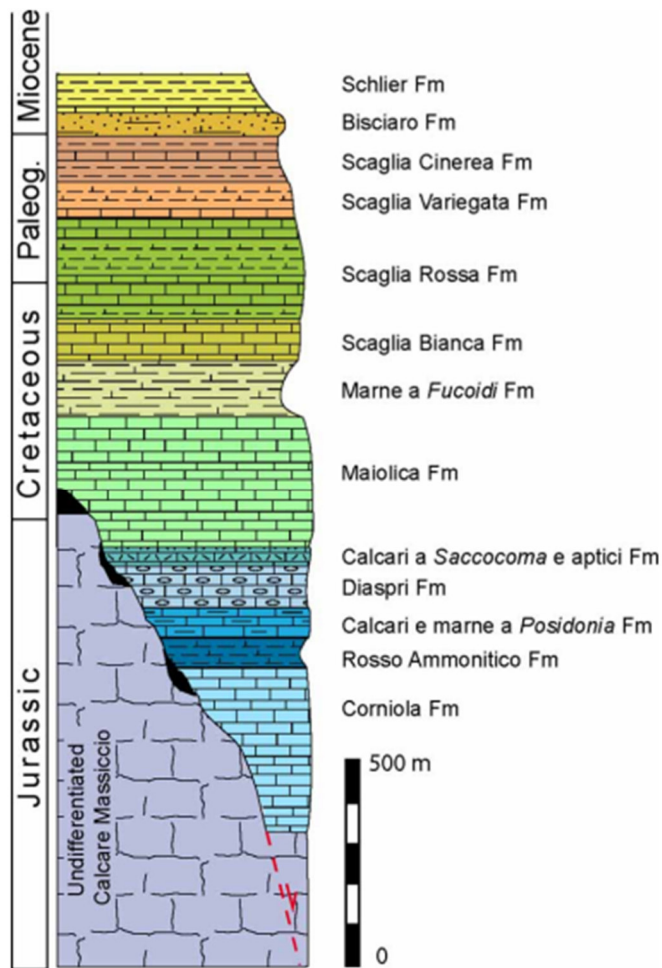
Figure 35. Umbria-Marche stratigraphic succession outcropping in Pioraco municipality (modified from Fabbi, 2015).

The Calcare Massiccio formation (Figure 36) has a large thickness, around 700-800 meters, and it is made of Early Jurassic limestone of elevated purity ($CaCO_3 > 98\%$) stratified in big banks. The Calcare Massiccio has a high permeability due both to the syngenetic porosity and to the strong set of fractures and faults cutting the banks. In the upper part the formations are slightly cemented with an elevate intergranular porosity. For this reason it accommodates the largest aquifers of the region (Paggi et al., 2017).

Figure 36. The Calcare Massiccio Fm. in the surroundings of Pioraco (modified from Paggi et al., 2017).

Pelagic-Jurassic deposits are a set of well stratified rocks of various lithology and thickness due to the synsedimentary extensive tectonic. Two main successions are usually identified, complete and condensate successions. Complete successions are formed by Corniola (Figure 37), Rosso Ammonitico, Calcari a Posidonia and Calcari Diasprigni Fms., made of marly and siliceous limestone with a thickness of hundreds of meters. The Corniola formation is made of highly stratified limestone with medium-high permeability due to the fracturing degree. The Corniola is in hydraulic connection with the underlying Calcare Massiccio Fm, in contact for stratigraphic succession or tectonic contact by synsedimentary faults. Marls of Rosso Ammonitico and other low permeability layers, belonging to the upper part of Calcari Diasprigni, block the hydraulic continuity between the set Calcare Massiccio-Corniola and the overlying calcareous unit (Maiolica Fm). Condensed successions are characterized by smaller thickness, less than 50 meters; they are formed mainly by stratified limestones highly compacted and slightly permeable, with the local presence of marly and siliceous levels.

Condensed successions constitute a barrier for permeability located between the Calcare Massiccio Fm and the Maiolica (Paggi et al., 2017).

Figure 37. Outcropping of Corniola Fm. around Pioraco (modified from Paggi et al., 2017).

The rocky substrate is covered by Quaternary fluvial-lacustrine deposits placed along the Potenza River and Scarzito River valleys. Other common covering layers in the area of interest are travertine, in correspondence of Pioraco city centre, slope debris, conoid of debris and alluvial fan.

For what concerns the geomorphology of the study area, the territory around Pioraco presents from the geological aspect two lithologies that may be distinguished considering the outcropping lithotypes, the geostructural condition, the hydrogeological behaviour and the morphology (Fabbi, 2015). The first is the west-central ridge made of limestones and marly limestones, where Pioraco is located; the second on the east side is hilly and characterized by pelitic and arenaceous substrates where Seppio and Paradiso are located (Fabbi, 2015). As shown in Figure 38, the E/W trending Potenza river valley and the SSW/NNE trending valley of the Scarzito River (which joins with the Potenza river at Pioraco) separate three main ridges (Mt. Primo, Mt. Gualdo and Mt. Castel Santa Maria) (Fabbi, 2015). The higher elevations

exceed 1000 m (Mt. Primo, 1299 m; Mt. Castel Santa Maria, 1238 m), while the valley bottoms lie at an average elevation of 400– 500 m asl (Fabbi, 2015).

Figure 38. Panoramic view of the Mt. Primo and Mt. Gualdo ridges from Mt. Castel Santa Maria (modified from Fabbi, 2015).

In this portion of the Apennines, a regular pattern of NNW-SSE aligned anticlines and subparallel synclines was produced by the mountain chain building and controls the distribution of ridges and valleys in the present day topography (Cresta et al., 1989). Nevertheless, prior to being involved in the mountain chain building, the area was affected by a major extensional phase in the Early Jurassic, resulting in a submarine paleotopography which would produce a strong lateral variability of facies and thickness in the carbonate succession during the remainder of the Jurassic (Fabbi, 2015). The valley floor is bordered by rock walls of the Calcare Massiccio Fm. and Corniola: these rock masses are stratified and present discontinuities (faults, shear and cleavage stress fractures) with orientation, spacing and frequency, opening and mechanical characteristics such as to imply potential rockfall, toppling or flow (Hoek & Bray, 1981; Goodman and Bray 1976). These types of motions are particularly dangerous in proximity of sub-vertical slopes (Fabbi, 2015). Figure 39 shows the geological interpretation of the Mount Castel Santa Maria (Fabbi, 2015).
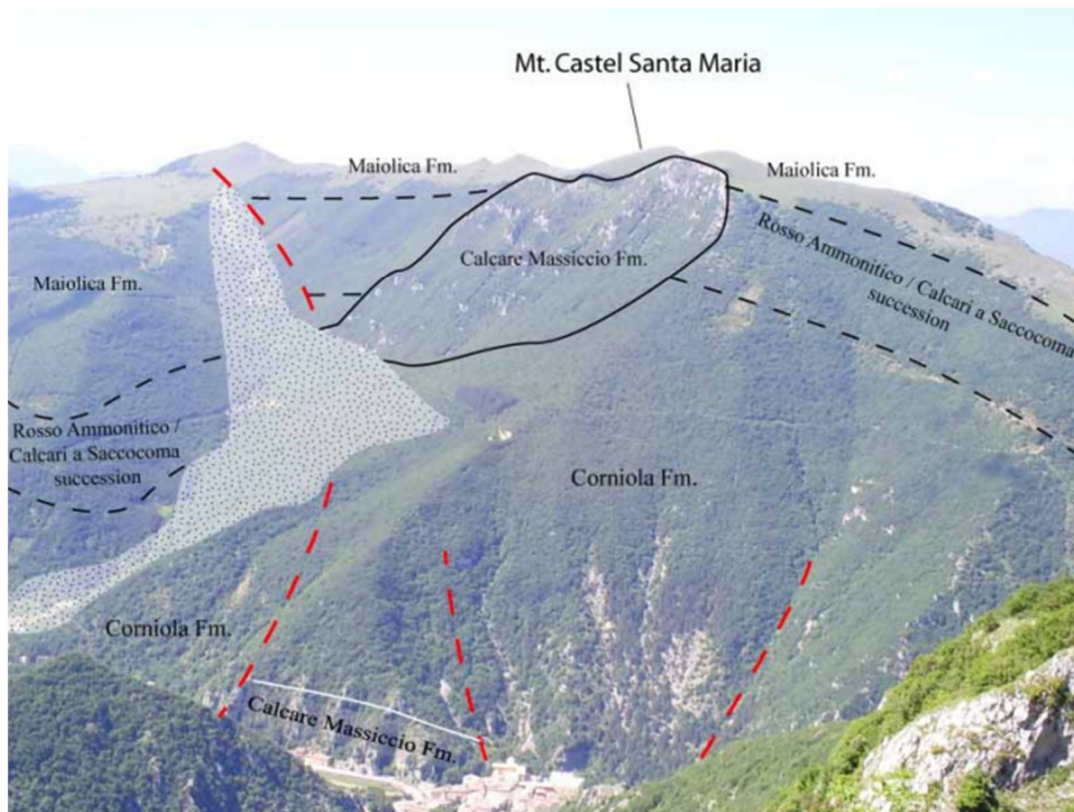
Figure 39. Geological interpretation of the southern slope of Mt. Castel Santa Maria (modified from Fabbi, 2015).

Along the valley of Scarzito River and Potenza River, close to the Pioraco cave, there are gullies filled by debris flows that are usually activated by severe climatic events such to generate debris fans at the bottom of slopes (Paggi et al., 2017). In the last years, the frequency of this phenomenon has progressively decreased in relation with growing and spreading of vegetation along the slopes. .

3.2 Hydrogeology of the study area

As described in the chapter concerning the geological description of the area around Pioraco, the Madonnetta district stands above clayey alluvial fluvial-lacustrine deposits lately formed, with a thickness ranging from zero to fifty meters (Paggi et al., 2017). This geological unit is bounded at the bottom and laterally by fluvially originated gravels that accommodate an aquifer fed by carbonate structures. The clay deposit is made of fine fraction, silt and clay, with low permeability. The gravel bank is highly permeable as well as the substrate, featured by elevate porosity (accounting for primary permeability), severe fracturing degree and

chemical dissolution (accounting for secondary permeability). The strong degree of fracturing identified on the geological formations present in the study area promotes an intense underground hydric circulation, also linked to the permeability characteristics of the outcropping lithologies (Galdenzi, 2019).

Inside the carbonate succession three main permeable hydrogeological complexes can be identified, Calcare Massiccio, Maiolica and Scaglia group (Figure 40), separated by two main aquicludes (Jurassic complete succession and Marne a Fucoidi) (Galdenzi, 2019).
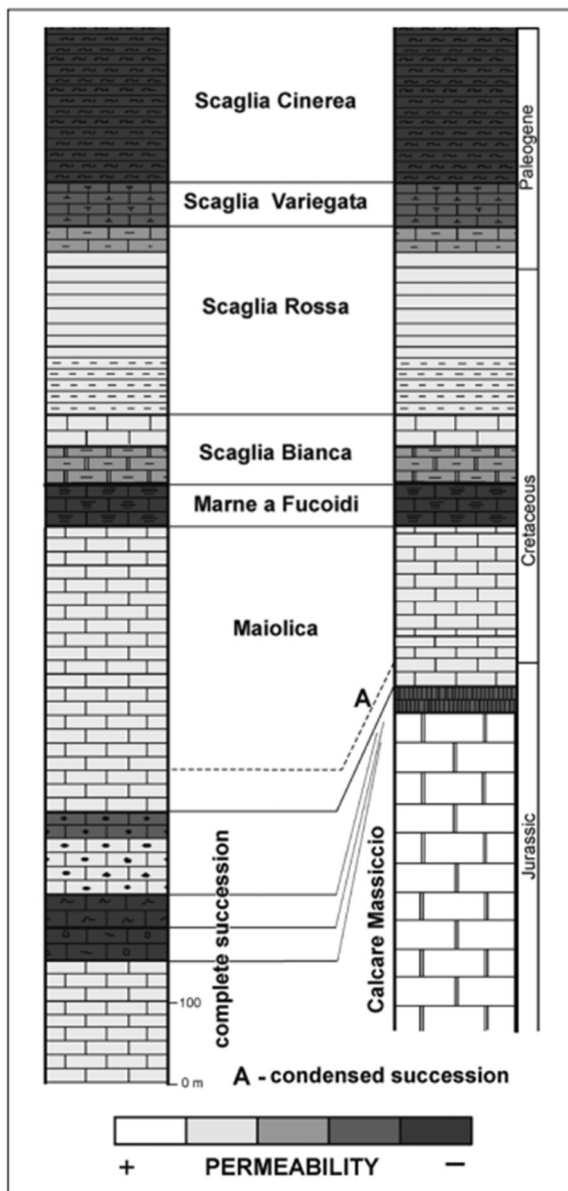

Figure 40. Schematic stratigraphic succession, with qualitative permeability of the different units (modified from Galdenzi, 2019).

Galdenzi et al. (2019) carried out a study on the cave and karst water around the Monte Lago karst plains (Central Apennines) that has revealed an articulate drainage pathway, influenced by the karstification degree and geological setting. The study investigated the influence of geologic structure and degree of karstification on groundwater drainage in the area around Pioraco and revealed an articulate drainage pathway starting from Monte Lago plain ponor, a natural surface opening typical of karst landscape (Galdenzi, 2019). Subterrain water circulation in soluble rocks, such as limestones, are deeply linked to karst processes which determine an expansion for chemical corrosion of pores and consequently an increase permeability and runoff velocity (Galdenzi, 2019). It was assessed that the permeability inside the same geological unit does not depend only on the lithological characteristics, but varies locally due to the different degree of karstification that has been reached over time (Galdenzi, 2019). The presence of low permeability marls within the sedimentary succession forces the formation of aquifers inside the different hydrogeological complexes. Despite the alternance of aquicludes, the cutting from the set of both compressive and distensive faults allows to create hydraulic connections between aquifers, complicating the subterrain pattern (Figure 41) (Galdenzi, 2019). Small aquifers with local importance develop inside the single hydrogeological complex but also regional aquifers, fed by formations belonging to different hydrogeological units and extended to a bigger section of geological structure (Galdenzi, 2019).
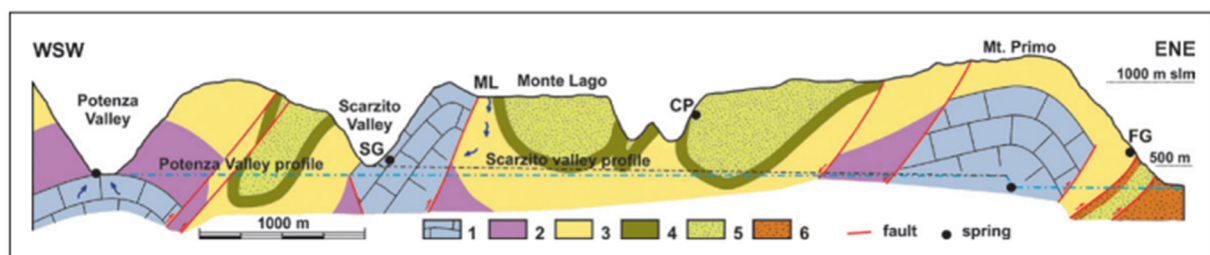

Figure 41. Hydrogeological scheme of the area. Legend: 1) Calcare Massiccio; 2) Jurassic Fms. 3) Maiolica; 4) Marne a Fucoidi; 5) Scaglia; 6) Oligocene and Miocene marl (modified from Galdenzi et al., 2019).

4. Materials and methods

The aim of this study is investigating the hydrogeological, geo-structural and geophysical features of the zone around Pioraco as support for geotechnical modeling of the clay consolidation processes.

Together with an accurate literature review about the geological characterization and the main hydrogeological features of the Madonnetta district (Figure 42), the study includes several field surveys and the following tests and analysis:

1. set, download and interpretation of the piezometric measurements, to control the variation of groundwater table;

2. tracer tests, to retrieve the permeability values of soil and find out the major pathways for groundwater flow;

3. rainfall analysis, to determine and quantify the relationship between rainfall and groundwater level variation rate.

Figure 42. Overview of the Madonnetta district of Pioraco village (modified from Lenci, 2021).

The purpose is monitoring the groundwater level inside the piezometers to understand the direction of the groundwater flows and how the porosity and permeability features of different geological units affect the motion. This result is achieved using divers, which are essentially dataloggers able to record in continuous and independently the water level rise and drop, the electric conductivity of water, the pressure. Figure 43 shows the divers

catalogue of the Eijkelkamp company, one of the world's leading company in the environmental monitoring field (https://www.royaleijkelkamp.com/search/?q=diver).

Figure 43. Diver catalogue by Eijkelkamp company.

Tracer tests are meant to provide an estimation of the permeability value of the gravel layer to reveal viable drainage paths for groundwater through the layers.

The analysis of precipitation is carried out to have a complete scheme of the relationship between rainfall amount and the water level in the aquifer. The precipitation data were downloaded from Protezione Civile of Marche Region website (http://app.protezionecivile.marche.it/sol/indexjs.sol?lang=it) as base to evaluate the relationship between the rainfall amount and the variation of the water head inside each piezometer in the area of interest.

4.1   Piezometric level monitoring

The hydrogeological framework of the area is characterized by an aquifer represented by the gravel layer and fed by local precipitations and, partly, by the high permeable carbonate structures, Calcare Massiccio and Corniola Fms. Located at the basis of the gravel aquifer. The Potenza River results suspended on the aquiclude formation of silty clays (Lenci, 2021).

The measure of piezometric levels was performed in four different days, covering a period of 5 months, focusing mainly on the three piezometers PZ1,S4 and S5 (Figure 44 and Figure 45) that may be placed in correspondence of a preferential pathway for groundwater circulation as revealed by the isopleths map. The existence of a preferential flow path was hypothesized by observing the water displacement, amplified by the pumping operation started in 2009, towards the PZ1-S4 direction.
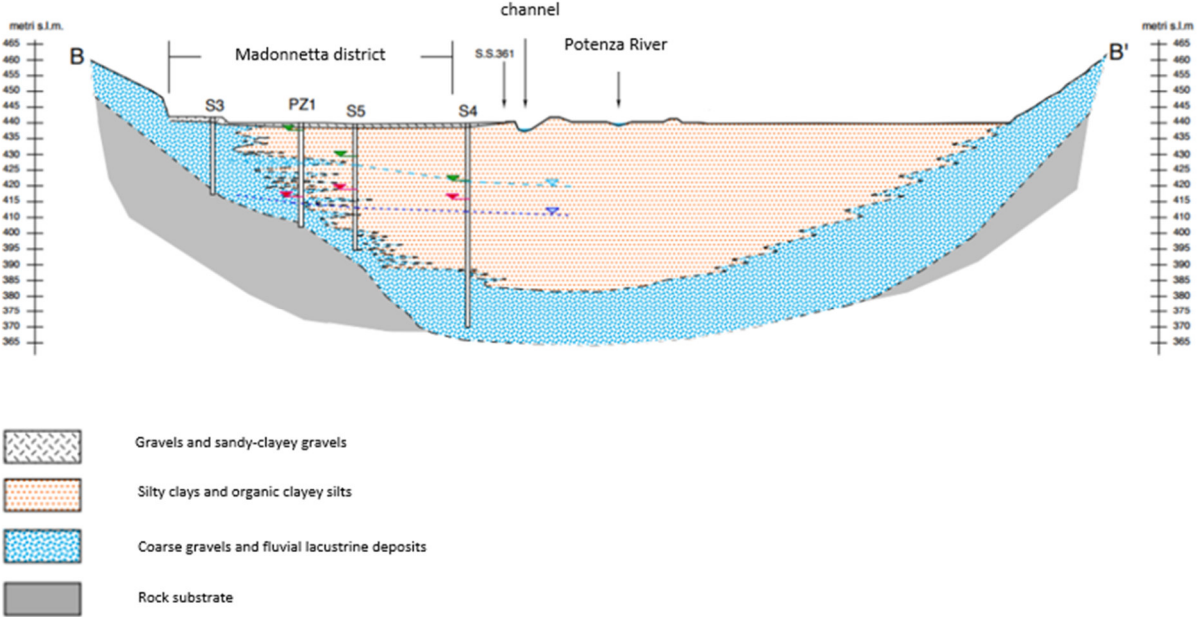

Figure 44. Installation of piezometers and depth along the section North-South (modified from Lenci, 2021).
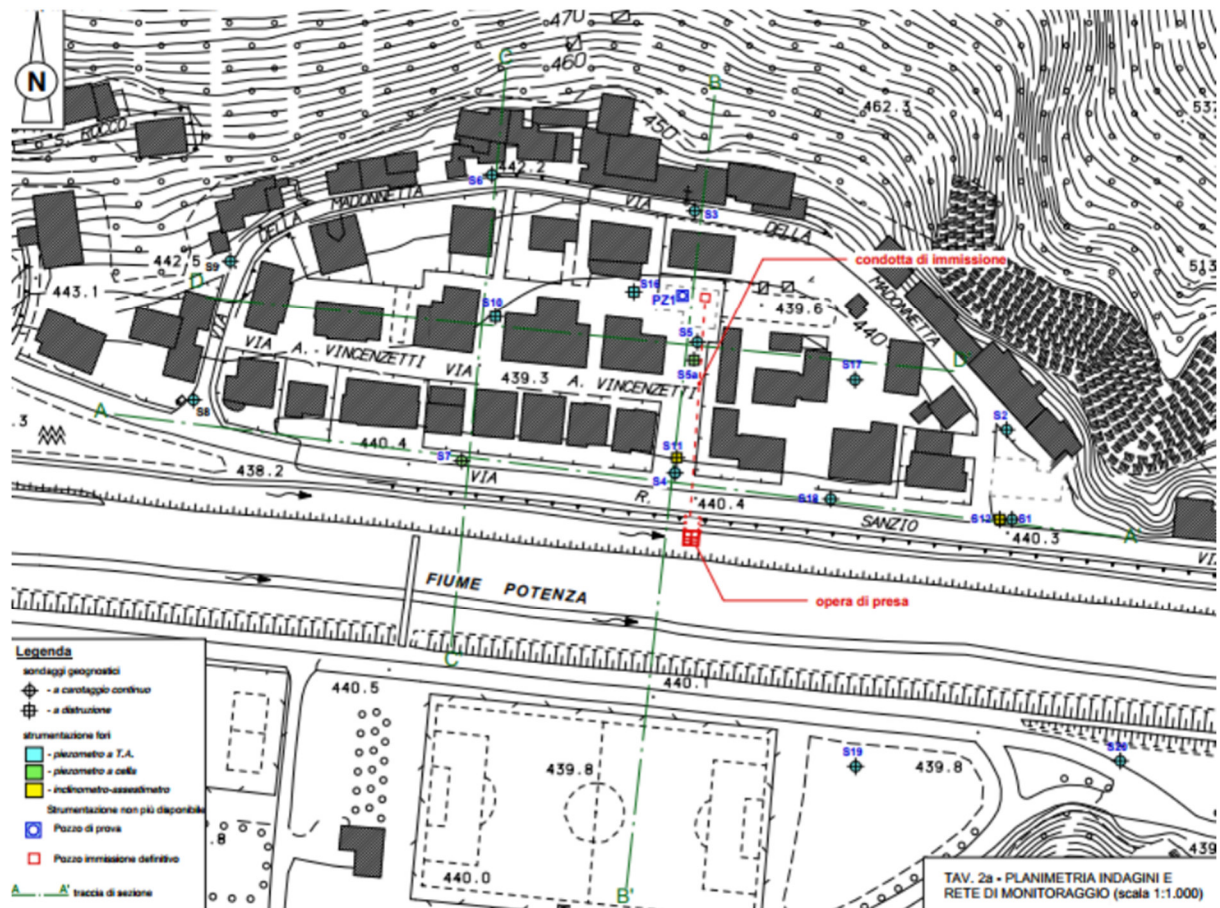
Figure 45. Location of stratigraphic sections and piezometers (modified from Lenci, 2021).

The measures are made using a phreatimeter, also known as water level indicator; this instrument is made of a retractable graduated rod with a sensor which emits an acoustic signal once it gets in contact with the water table, providing the water level from the ground level (Figure 46).

Figure 46. Setting of the diver into piezometer S4, measure of water level and electric conductivity, July 2021.

4.2   Tracer test

On July 21st at 12:00:00 we performed a tracer test to assess the permeability of the deposit layer that accommodates the main water flux. As shown in Figure 47, twelve kilograms of sodium chloride (NaCl) were dissolved in 335 litres of water and the solution was poured inside the piezometer PZ1, the northernmost. The expected result was recording with divers an increase of concentration in the downstream piezometers, in order of time initially in S5 and later in S4. On August 30th, the day of the next survey, we downloaded the data collected in each well by divers to evaluate the concentration variation over time due to the tracer advection in the soil.

Figure 47. Sodium chloride dissolution in water for the tracer test, July 2021.

5. Results

5.1 Tracer test result

5.1.1 Break Through Curve

Figure 48 displays the concentration variation in three monitoring points, corresponding with PZ1 (injection point, black), S5 (14 m far from PZ1, blue), S4 (52 m far from PZ1, red). In particular, the concentration curve in PZ1 suddenly increases the same day of the injection (21/7/22) up to the value of 25.9 g/L then decreases until the disappearance in 27/7/22 at 19:43.
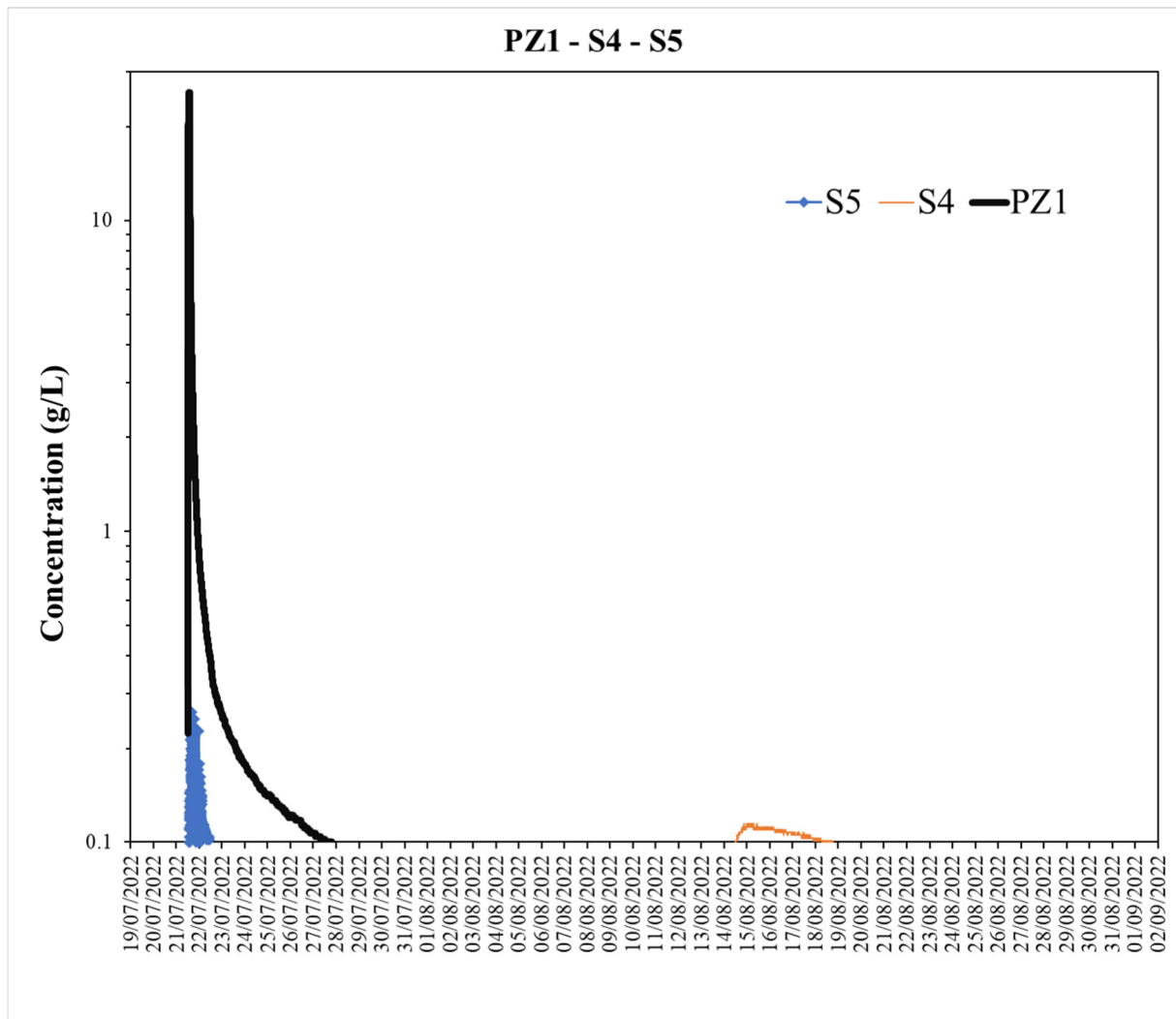

Figure 48. Concentration variation over time in logarithmic scale; data acquired though divers in PZ1, S5, S4 (our elaboration).

Starting from these data it is possible to calculate the minimum and maximum disappearance velocity (Table 6) by taking into account respectively the more flatten part of curve, the final section, and the steeper one, right after the tracer injection; these velocities correspond to flow or linear velocity of groundwater.

diameter (cm)	18	diameter (cm)	18
alfa	1,7	alfa	1,7
t i		t i	
t f		t f	
t (hours)	0,65	t (hours)	15,33333333
c in	25,9	c in	0,9985
c fin	9,08	c fin	0,3624
m	1,612567348	m	0,06609819
v f (cm/h)	13,41007871	v f (cm/h)	0,549671262
v max (m/d)	3,218418889	v min (m/d)	0,131921103
v max (cm/s)	3,73E-03	v min (cm/s)	1,53E-04

Table 6. Maximum and minimum disappearance velocity of tracer from PZ1 (our elaboration).

5.1.2 Average flux velocity PZ1-S5

As displayed in Figure 49, restricting the concentration variation graph up to the 28/7/22, the tracer arrived in S5 the same day of injection at 14:34 while it disappeared the day after at 11:30. Once defined the mass centre it was possible to determine the incoming tracer velocity so the average flux velocity between PZ1 and S5 (14m) (corresponding to the effective or actual velocity of groundwater).

PZ1 - S5
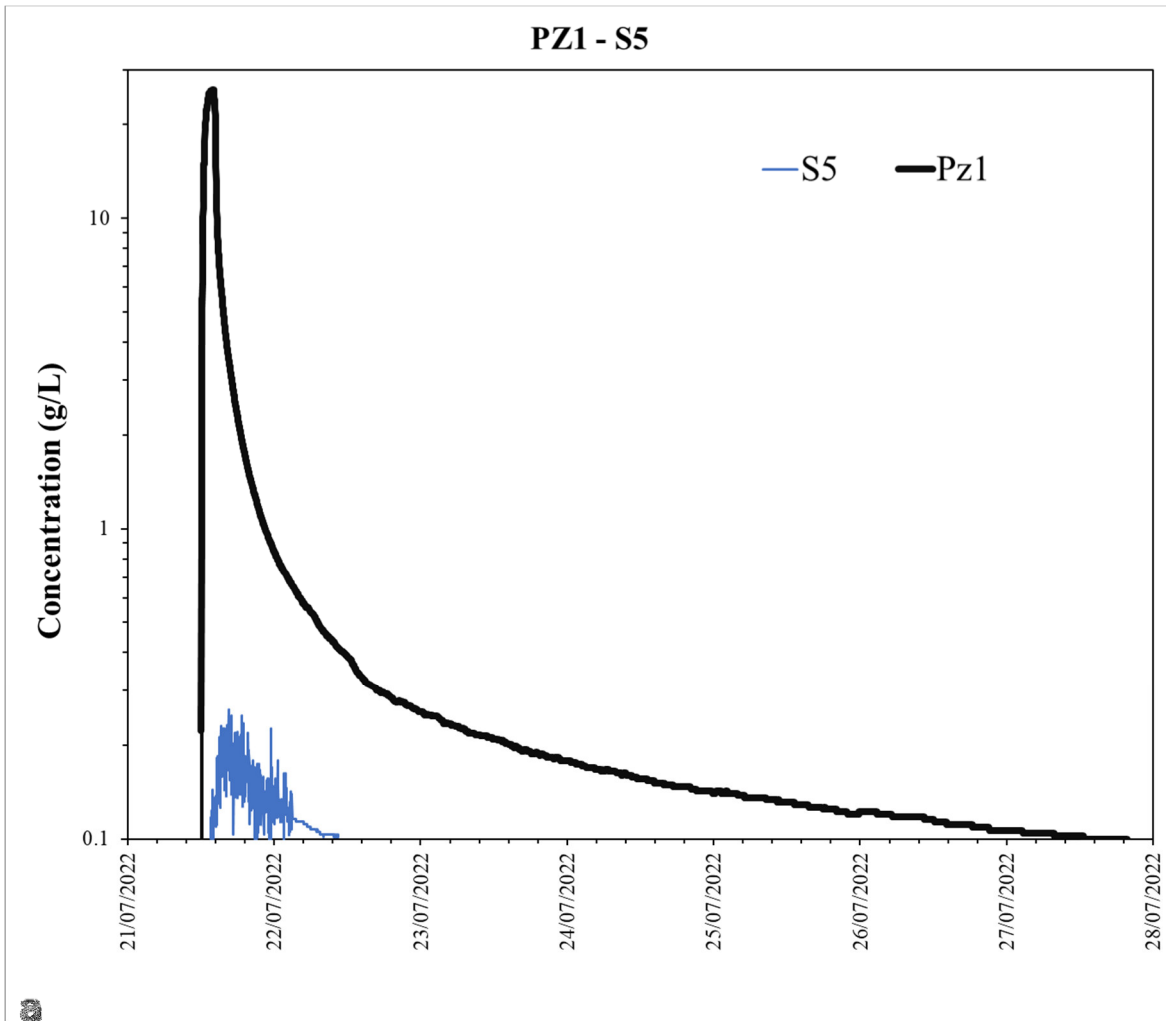
476.0	minutes
7.9	hours
0.3	days
28560	seconds
1.8	m/h actual velocity
0.000490196	m/s actual velocity
42.35	m/day actual velocity
4.90E-02	cm/s
0.50	gradient
9.80E-02	cm/s permeability

Figure 49. a) Detail of tracer recording in PZ1 and S5; b) permeability calculation (our elaboration).

5.1.3   Average flux velocity PZ1-S4

Focusing on the piezometer S4 shown in Figure 50, the tracer was recorded the 14/8/22 at 13:01 while it disappeared completely the 18/8/22 at 19:17. Calculating the mass centre we

could obtain the average flux velocity between PZ1 and S4 (52 m). Anyway this curve is not completely reliable since the concentration does not increase rapidly as clearly as in the other piezometers.
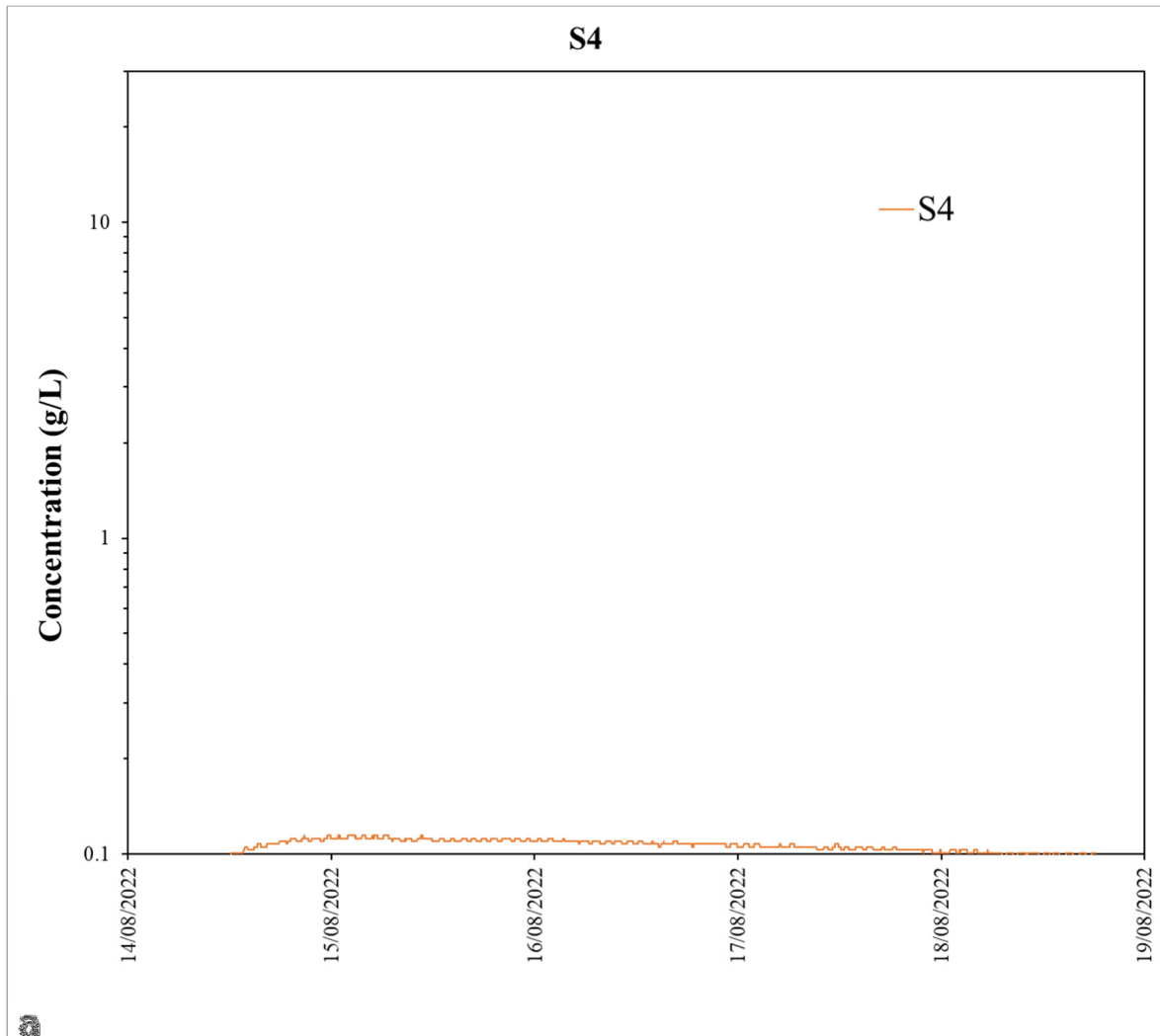
37594	minutes
627	hours
2255640	days
26,11	seconds
0,083	m/h actual velocity
2,31E-05	m/s actual velocity
1,99	m/day actual velocity
2,31E-03	cm/s
0,22	gradient
1,05E-02	cm/s permeability

Figure 50. a) Tracer recording in S4; b) permeability calculation (our elaboration).

5.1.4   Average flux velocity between S5-S4

Table 7 shows the calculation of the permeability value between the points S5 and S4.

37118	minutes
619	hours
2227080	days
25,78	seconds
0,061	m/h actual velocity
1,74E-04	m/s actual velocity
1,47	m/day actual velocity
1,74E-02	cm/s
0,11	gradient
1,58E-01	cm/s permeability

Table 7. Flux velocity calculated between S5 and S4 (our elaboration).

5.1.5   Hydraulic gradient calculation

For what concerns the gradient definition, we calculated the depth difference between PZ1-S5, S5-S4, PZ1-S4 and the distance between PZ1-S5, S5-S4, PZ1-S4. Then with the ratio *depth difference/length difference* we obtained the following values:

1. PZ1-S5: 0,5
2. PZ1-S4: 0,22
3. S5-S4: 0,11

5.1.6   Permeability calculation

The permeability of the medium crossed by the flux was estimated by considering the ratio *average flux velocity/gradient*:

1. PZ1-S5: $9,8 \cdot 10^{-2} \; cm/s$
2. PZ1-S4: $1,05 \cdot 10^{-2} \; cm/s$
3. S5-S4: $1,55 \cdot 10^{-1} \; cm/s$

5.1.7 Recap table

Tract	PZ1-S5	PZ1-S4	S5-S4
Distance	14m	52m	38m
Delta H	7m	11m	4m
Gradient	0,5	0,22	0,11
Arrival	21/07/2022 - 14:34	14/08/2022 - 13:01	----------
Disapperance	22/07/2022 - 11:30	18/08/2022 - 19:17	----------
Flux velocity	4,9E-02 cm/s	2,25E-03 cm/s	1,7E-02 cm/s
Permeability	9,8*E-02 cm/s	1,05*E-02 cm/s	1,58E-01 cm/s

Table 8. Flux velocity and permeability determination for the section PZ1-Z5, PZ1-S4, S5-S4 (our elaboration).

5.2 Piezometric levelling

5.2.1 Phreatimeter measures

In Table 9, the measures made from 18/5/22 to 12/10/22 are reported and show very different value for each piezometer. The largest gap is always recorded between PZ1 and S4: 12.6 m of difference in May, 5.5 m in July, 11 m in August and 12 m in October. The level of the piezometer S5 always falls inside the range PZ1-S4. Focusing on the piezometers S10, S16, S18, it is not possible to observe any trend but the available data seem consistent if compared to the others.

PIEZOMETER	PZ1	S4	S5	S10	S16	S18
18/05/2022	9	22.6	16	10.34	9.1	NA
21/07/2022	17.55	23	21.47	NA	NA	12.17
30/08/2022	13.4	24.66	20.94	NA	NA	12.97
12/10/2022	13.12	25.36	21.4	9.97	11.62	12.81

Table 9. Phreatimeter measures in the period 18/5/22 – 12/10/22 (our elaboration).

5.2.2 Piezometric map evolution

Five piezometric maps illustrating the difference between the piezometric level before and after the water injection in the pumping well are presented in Figure 51 and Figure 52. The blue lines represent the isopleths, the set of points with the same piezometric level (meters a.s.l. indicated in black). Map a) is from November 2nd 2004; map b) is from November 22nd

2007, both before the start of the pumping operation. The two maps show two zones of depression with the lowest values over the entire area: 414 m around S5 and 412 m around S4.
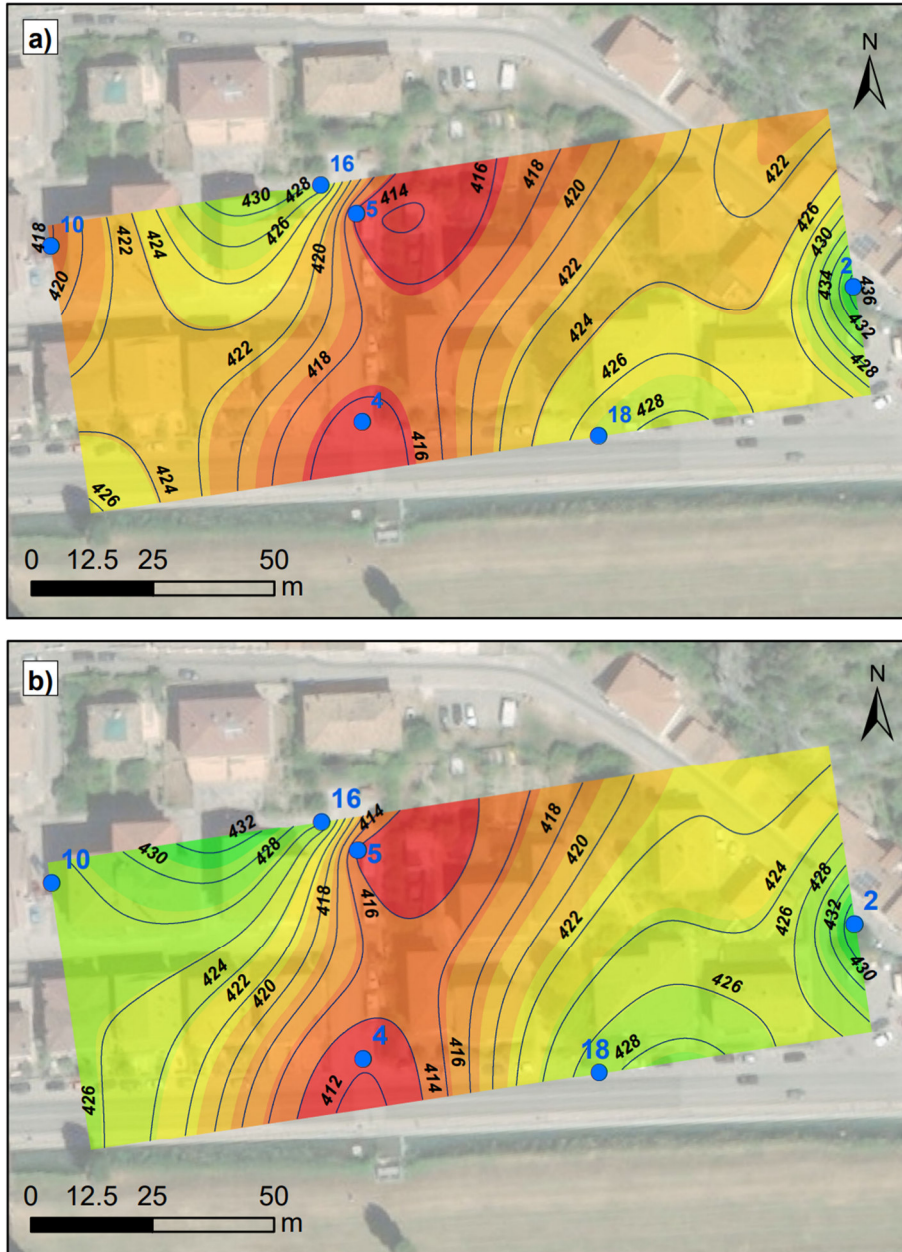

Figure 51. a) Piezometric map 02/11/2004; b) piezometric map 22/11/2007 (our elaboration).

Map c) is from November 23rd 2009 and map d) from October 11th 2022; they show over the whole map greater values of the water head than those measured before the water pumping. The level has increased up to 420 m around S5 as well as in S4, up to 418m, which

is still the lowest. Comparing map d) and c) there is a slight difference on the piezometric surface level which result lower in map d).
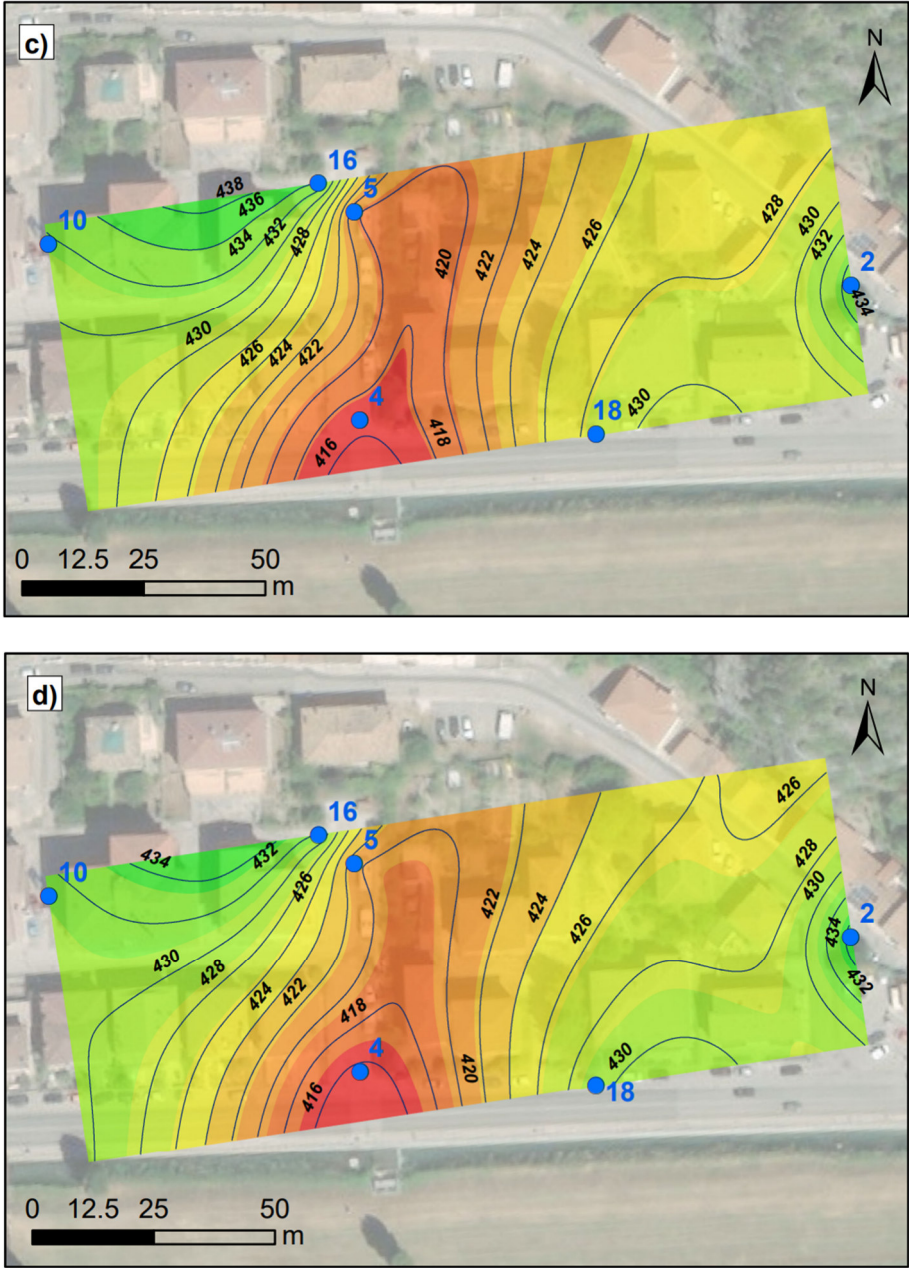
Figure 52. c) Piezometric map 23/11/2009; d) piezometric map 11/10/2022 (our elaboration).

5.3   Groundwater response to precipitations

The graphs below present the monthly cumulative of precipitations of four recording stations for the period January 2010-December 2021: Sorti (Figure 53), Camerino (Figure 54), Spindoli (Figure 55) and Esanatoglia (Figure 56). The largest amount of rainfall is recorded in

Sorti, which shows the highest values almost over the whole graph and the maximum value of 440 mm of water in November 2013.

Considering the average in eleven years, Sorti is the place with the highest monthly precipitations (125.7 mm), followed by Spindoli (107.4 mm), Esanatoglia (94.8 mm) and Camerino (78.9 mm). As expected in general, relevant precipitation values are related to the winter months for every stations.
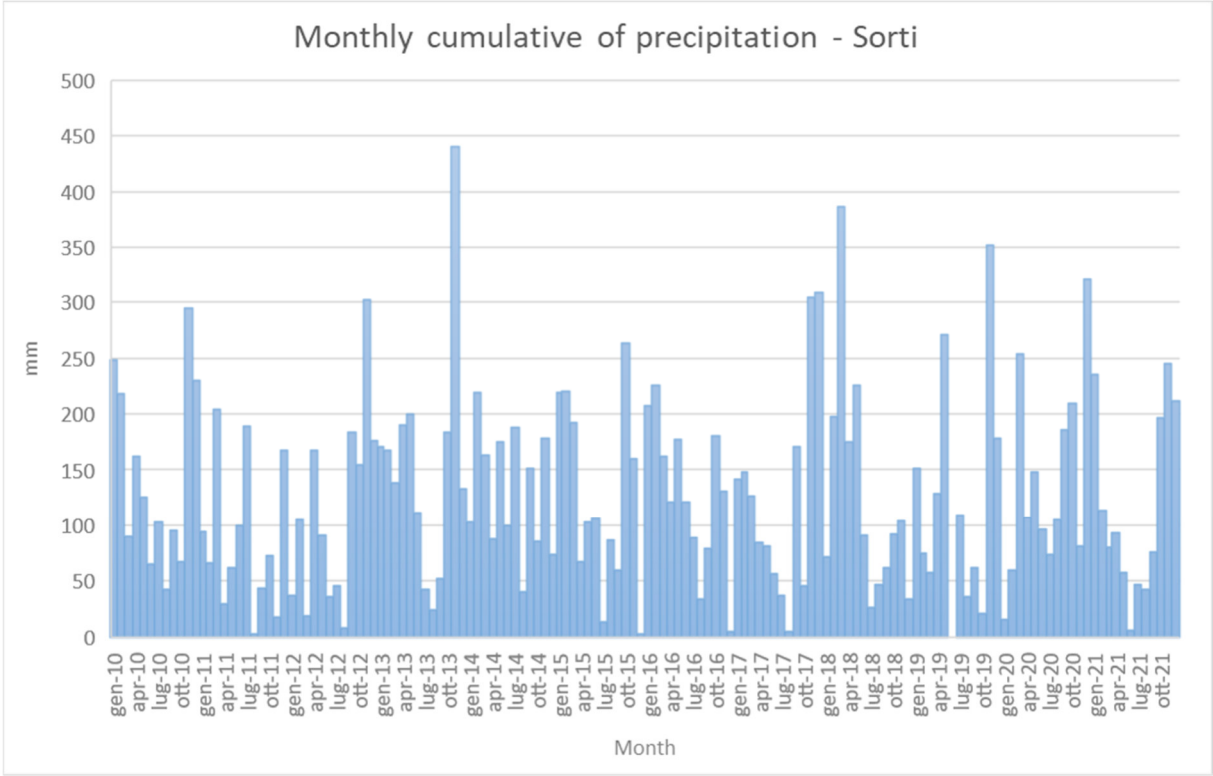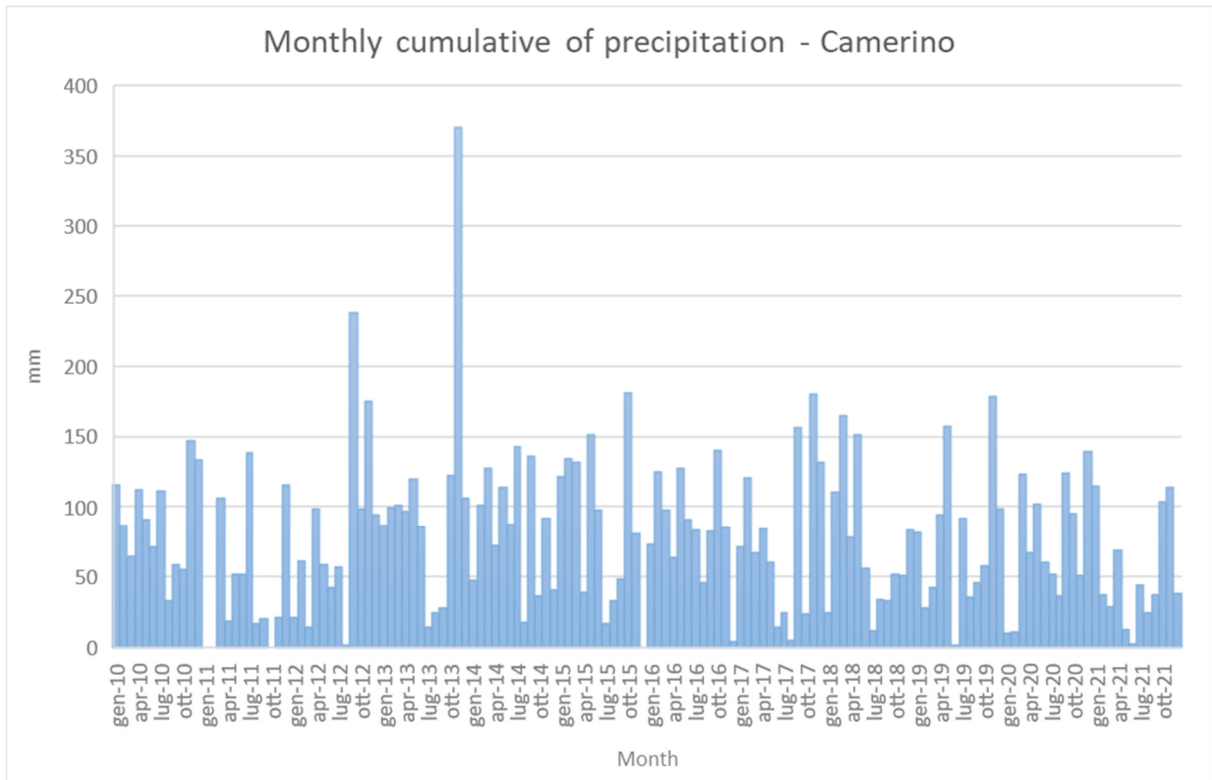

Figure 53. Monthly cumulative curves of precipitations recorded in Sorti (our elaboration).

Figure 54. Monthly cumulative curves of precipitations recorded in Camerino (our elaboration).
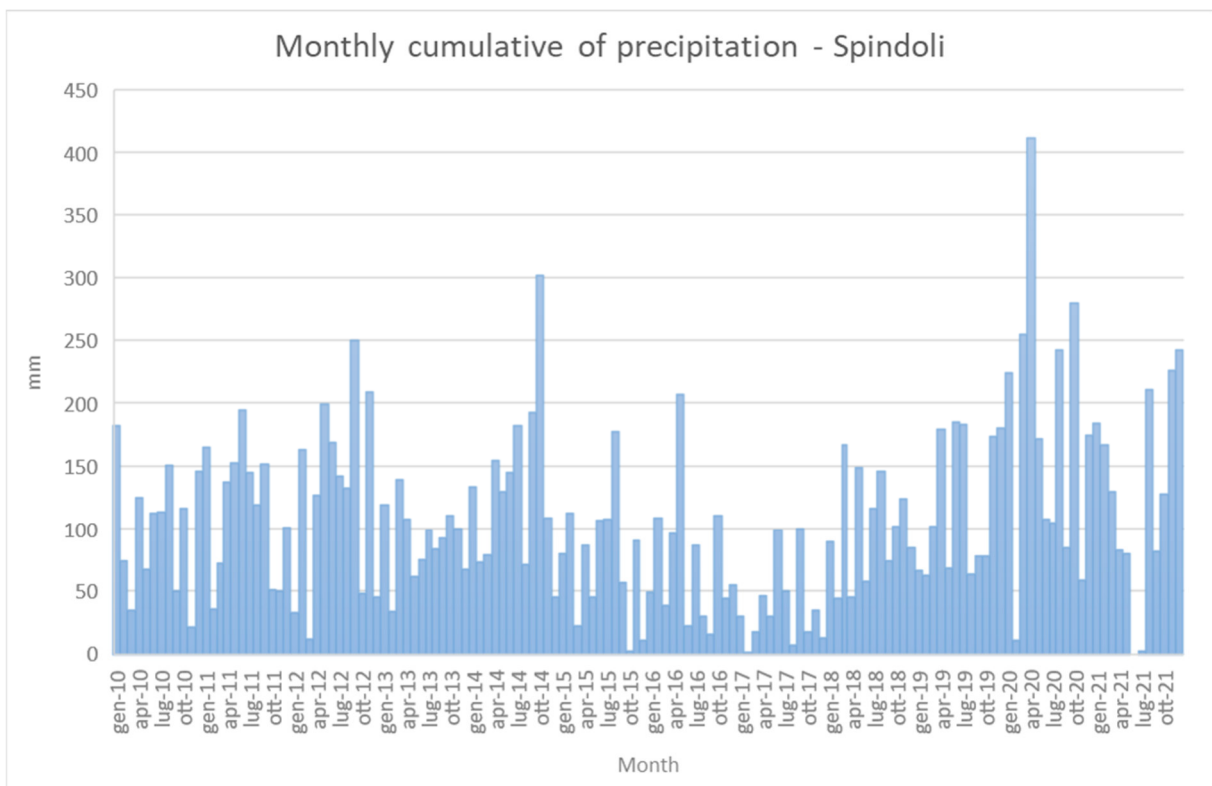

Figure 55. Monthly cumulative curves of precipitations recorded in Spindoli (our elaboration).
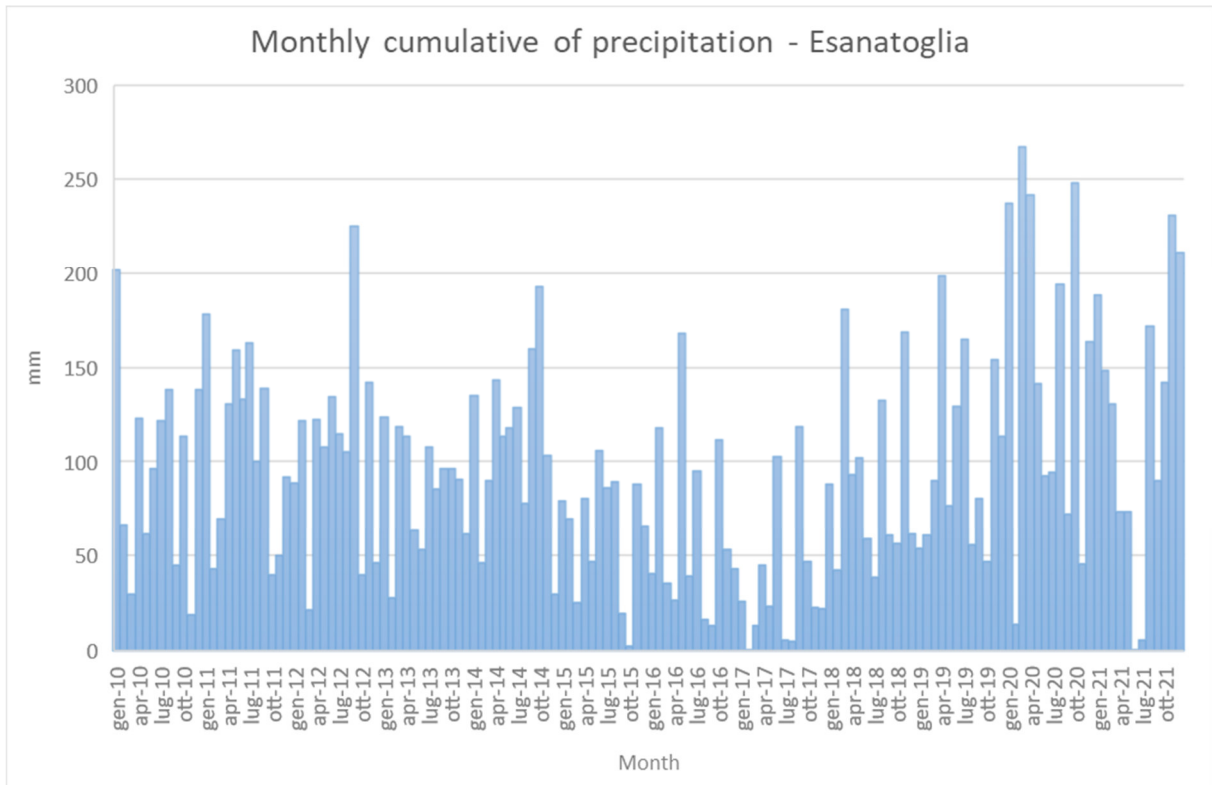
Figure 56. Monthly cumulative curves of precipitations recorded in Esanatoglia (our elaboration).

Figure 57 shows the precipitation analysis of Pioraco, displaying the daily cumulative precipitation on the vertical axis and the water head level in PZ1: the maximum value of daily precipitation (84.6 mm) occurs in September 21 and is followed by an abrupt rise in the piezometric level after a stable period. 21/07/2022-26/09/2022. The water head is measured with a diver and the displayed curve represents the variation of the water level (cm) above the diver for the entire observation period. The largest water head value is 13.77 m and the lowest 5.14 m.
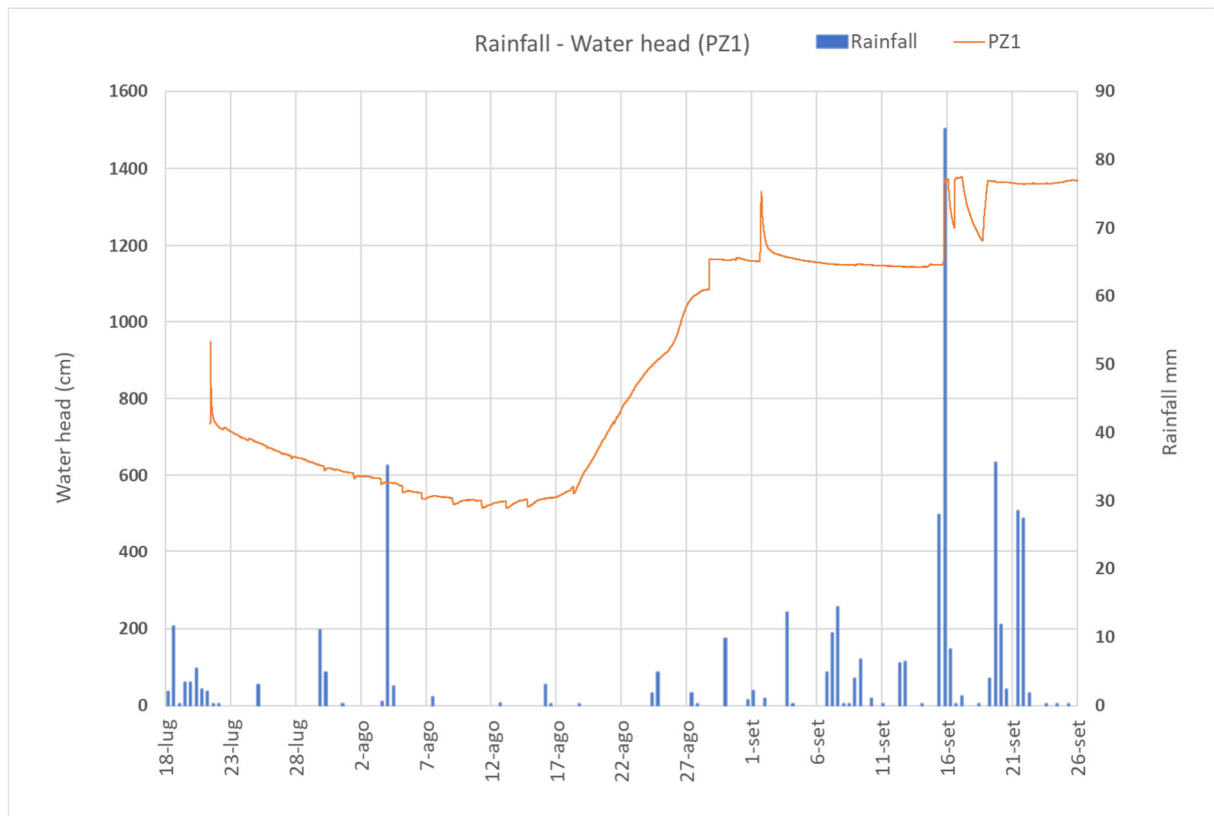
Figure 57. Daily cumulative of precipitation in Pioraco and the piezometric level in PZ1 (our elaboration).

On the other side, Figure 58 and Figure 59 display both the monthly cumulative of precipitations in Sorti and the water head variation for the piezometers S5 and S4, for which extended set of water head data are available (from 18/06/2021 to 26/09/2022). In S4, the maximum value of the water head is 3.63 m in June 2021, right before a decreasing trend. In S5, the maximum value is 4.70 m in June 2022. The monthly cumulative of rainfall shows high values in correspondence of the fall-winter months but reaches the largest value (279.4 mm) in August 2022.
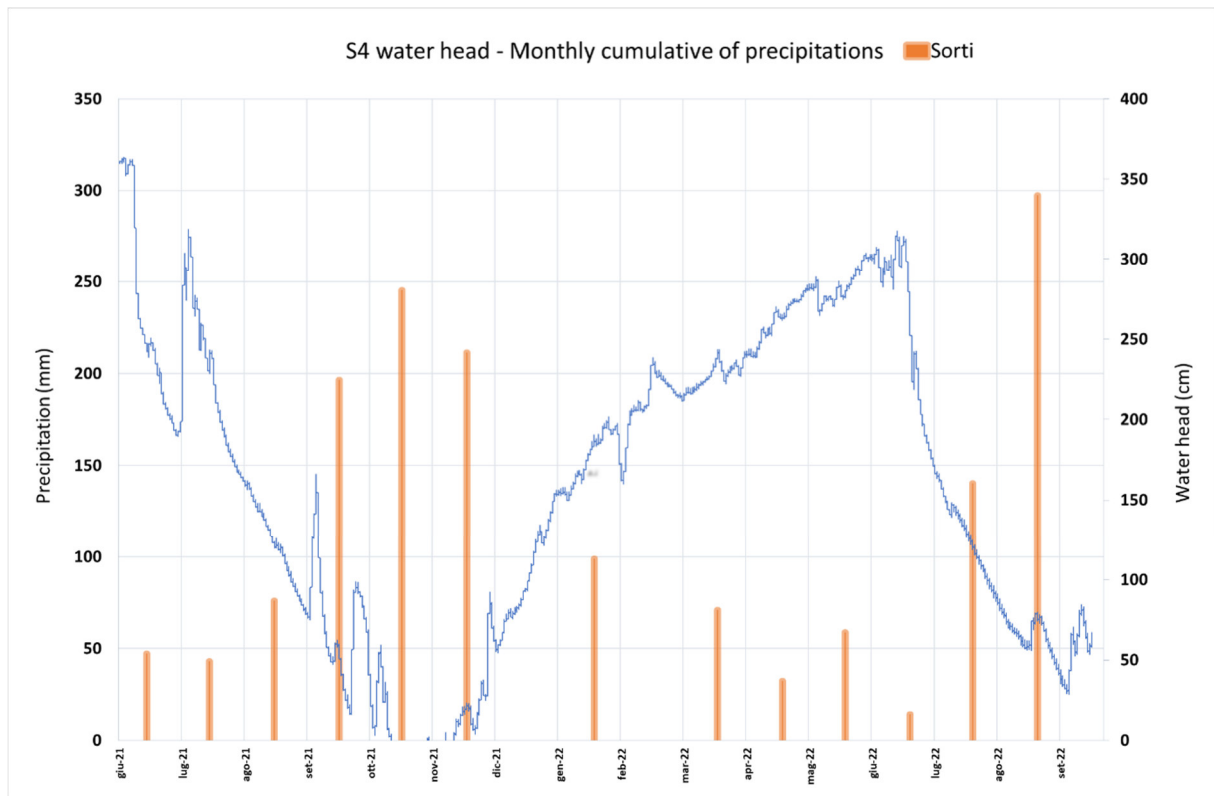
Figure 58. Precipitation cumulative curves and piezometric level variation in S4 (our elaboration).
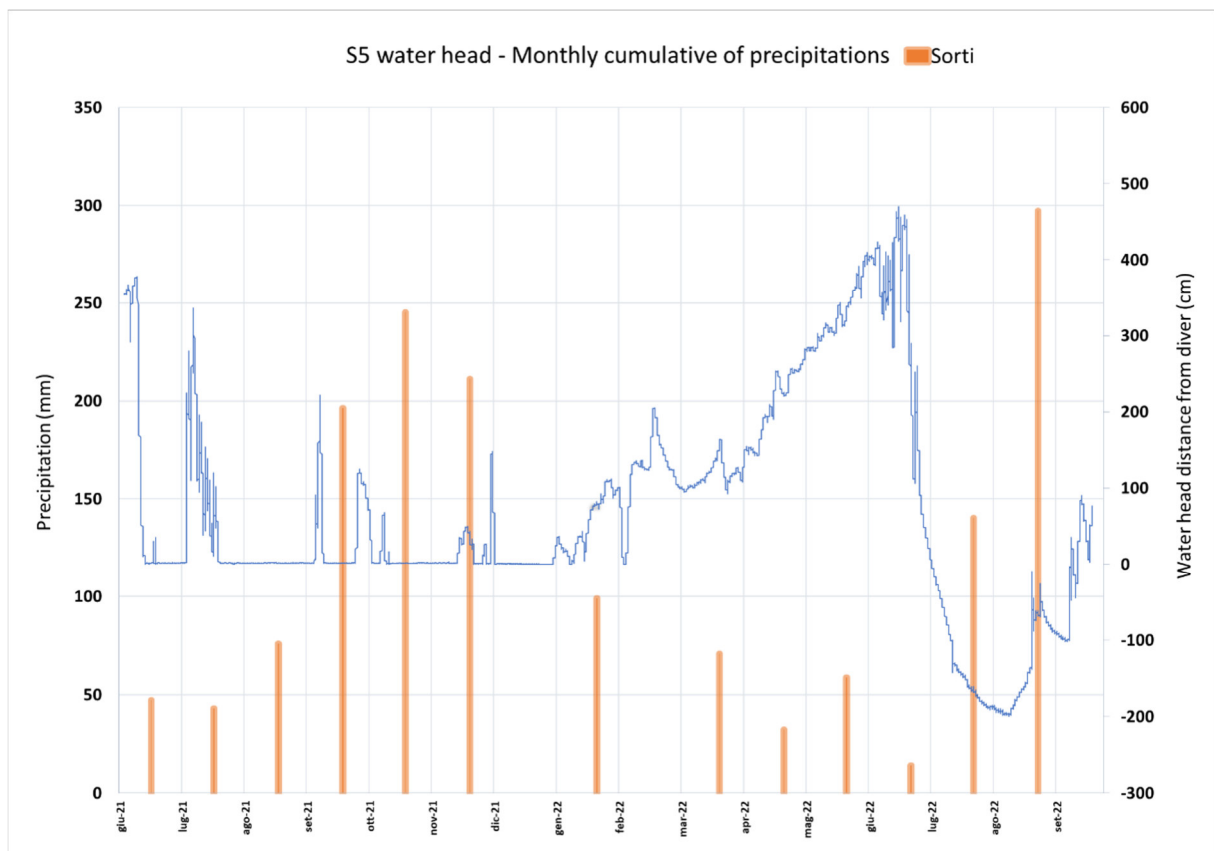

Figure 59. Precipitation cumulative curves and piezometric level variation in S5 (our elaboration).

Finally, Figure 60 provide a comparison of the water head of piezometers PZ1, S4, S5 and the daily cumulative of precipitations recorded in Pioraco from 21/07/2022 to 26/09/2022. The most severe daily precipitation (84.6 mm) occurred in 16/09/2022 while less intense rainfalls are regularly spread throughout the period.
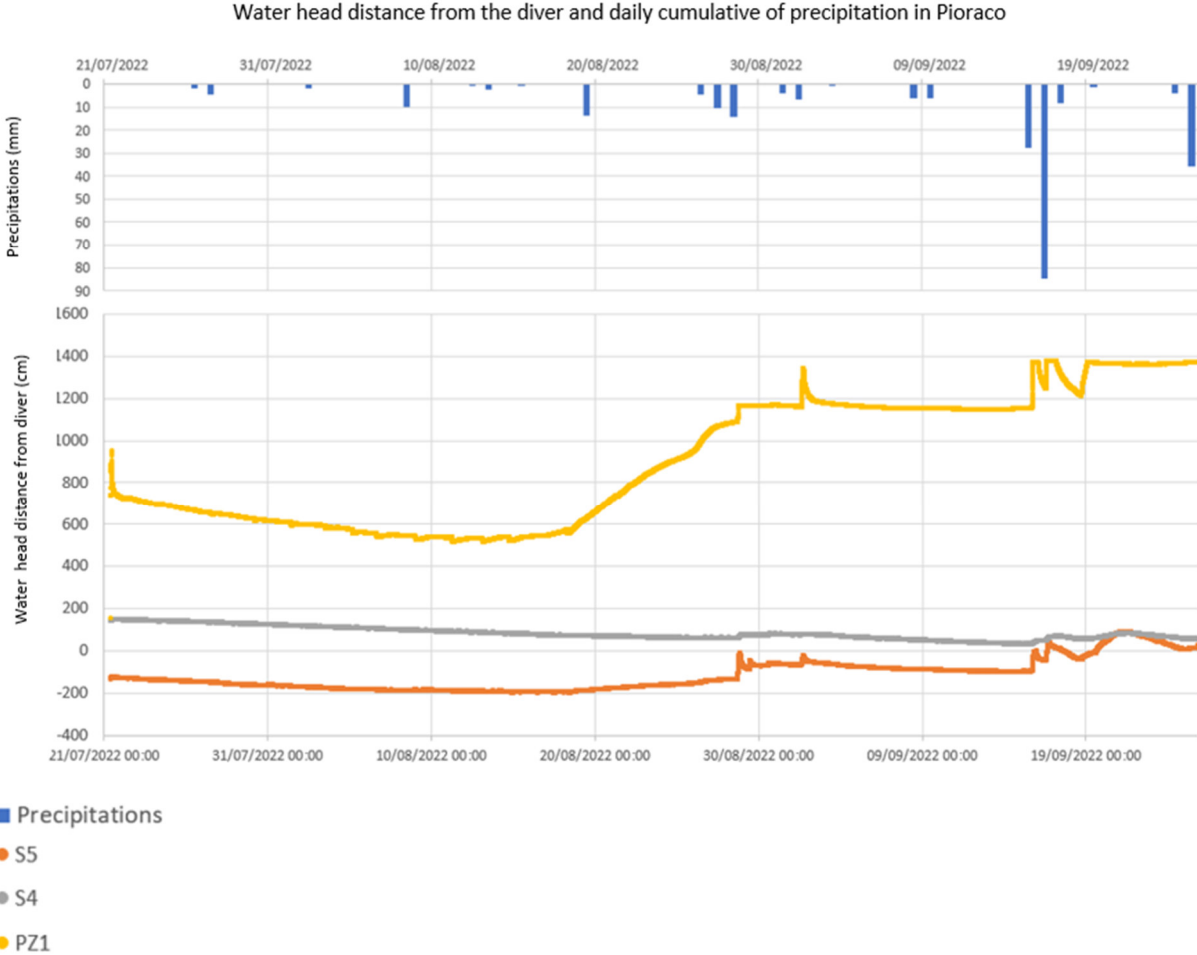

Figure 60. Water head distance from the diver and daily cumulative of precipitation in Pioraco (our elaboration).

6. Discussion

Figure 61 shows the geological cross section N-S directed in correspondence of the piezometers PZ1, S5, S4. Figure 62 instead, shows the installation point of the piezometer that will cover the main role for the discussion of the water drainage scheme.
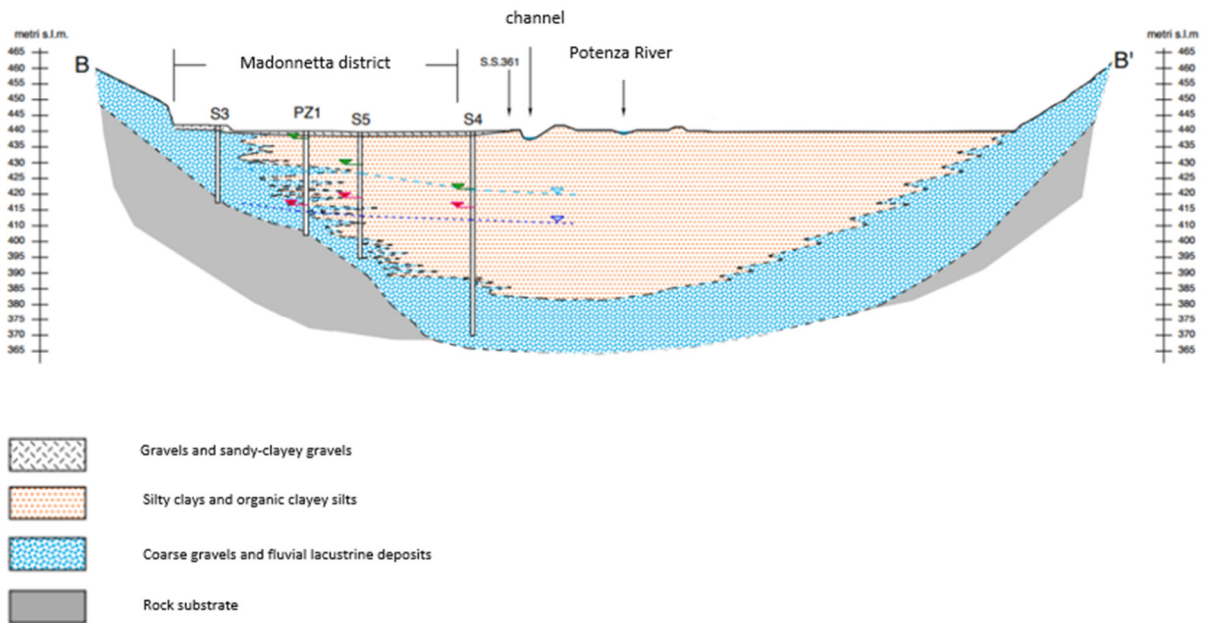

Figure 61. Installation of piezometers and depth along the section North-South (modified from Lenci, 2021).
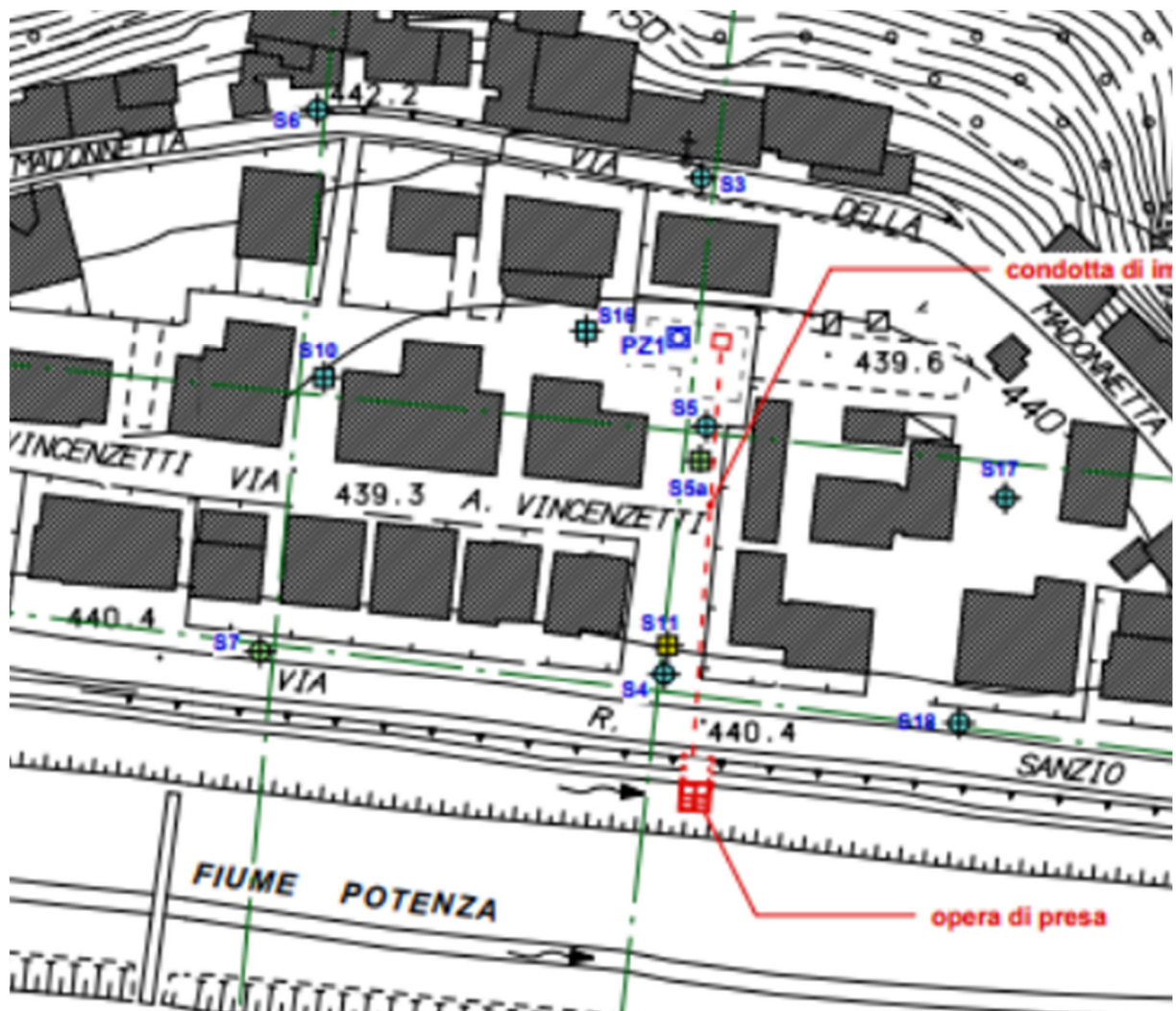
Figure 62. Piezometers location in the Madonnetta district (modified from Lenci, 2021).

The water head variation monitoring from years 2004 to 2022 have revealed a strong influence on the piezometric level due to the pumping operations.

Observing the piezometric maps concerning the period before the pumping operations (Figure 51), two depression zones located close to the piezometers S4 and S5 (Figure 62) are clearly identified. These zones result as two preferential convergence points of groundwater, both for water fluxes moving E-W and W-E. The entire zone between piezometers S5 and S4 results depressed in respect to the closer areas. This configuration of the piezometric surface in relation to the geological-stratigraphic condition highlights the existence of a possible preferential drainage pathway, which seems directed N-S. Considering the geological and

structural background, this direction results consistent with the presence of a regional normal fault outcropping in the rocky walls of the valley and buried by the thick layer of alluvial materials of the Potenza River. In addition, this fault has promoted the development of a small valley at the hydrographic left of the Potenza River which is responsible of the transport of the coarser and heterometric slope debris along its direction. It is possible to state that the preferential drainage direction is affected by the tectonic and stratigraphic conditions which do not depend on the water pumping operations.

After 2009, the area was interested by the general increase of the water head due to the continuous amount of water provided to the aquifer (Figure 52). The zone close to the injection well (around PZ1 and S5) has experienced a significative increase of the groundwater level; on the contrary the piezometer S4 seems to be less sensitive to the pumping because of the distance from the injection point. The piezometric map of 2022 (Figure 52 b) reveals a piezometric surface drop all over the zone due to the limited meteoric recharge that is characterized by a decreasing trend of precipitation (Figure 53).

Figure 63 shows the piezometric surface variation after the water pumping: it is possible to see that the largest rise occurred in the northern part of the area, around the piezometer S5, S10, S16, with gap of 6-7 meters. The variation peak of 7 meters is reached in correspondence of points close to the injection well. The water level in the zone around S4 and S18 has increased by 2-4 meters.
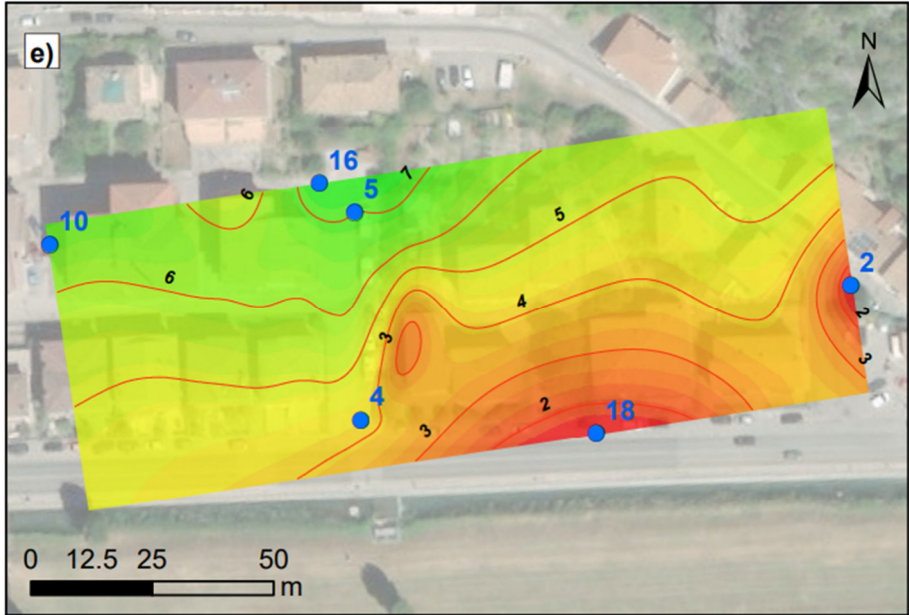

Figure 63. Map of piezometric level increase as consequence of water pumping (our elaboration).

Comparing the curves of the water head in PZ1, S5 and S4 in relation to the amount of the precipitations, the curve of PZ1 seems the most sensitive to rainfalls, probably depending on the reduced thickness of clay layer that stands above the gravels where the piezometer is set. On the contrary, the curves of S5 and S4 are much more flattened but show the same peak of water head of PZ1. This condition is verified by the results obtained during the geotechnical investigation (Lenci, 2021). Tests on soil samples revealed values of vertical permeability for the clay layer around 10^{-10}-10^{-11} m/s, which permits to exclude the theory of a rapid aquifer recharge due to the precipitations, particularly in correspondence of the points where the thickness of the clay layer is larger. For this reason, the aquifer recharge is mainly attributed to the carbonate formations. The piezometer PZ1, that is the closest to the carbonate substrate, records the largest piezometric oscillation with respect to S5 and S4 where the contribute of the groundwater flux is reduced by the distance. Moreover, the influence of the clay layer on compaction processes is visible considering the prediction computed by the model implemented for the geotechnical investigation of the area. Relevant consolidation values (around 30 cm) were estimated for a prediction of the subsidence process for the year 2071 along a vertical section of the Madonnetta district (Figure 65. Vertical displacement prediction for the year 2071 (modified from Lenci, 2021). Largest values of subsidence are estimated in correspondence of the central part of the section where the thickness of the clay deposit is larger (Figure 65).
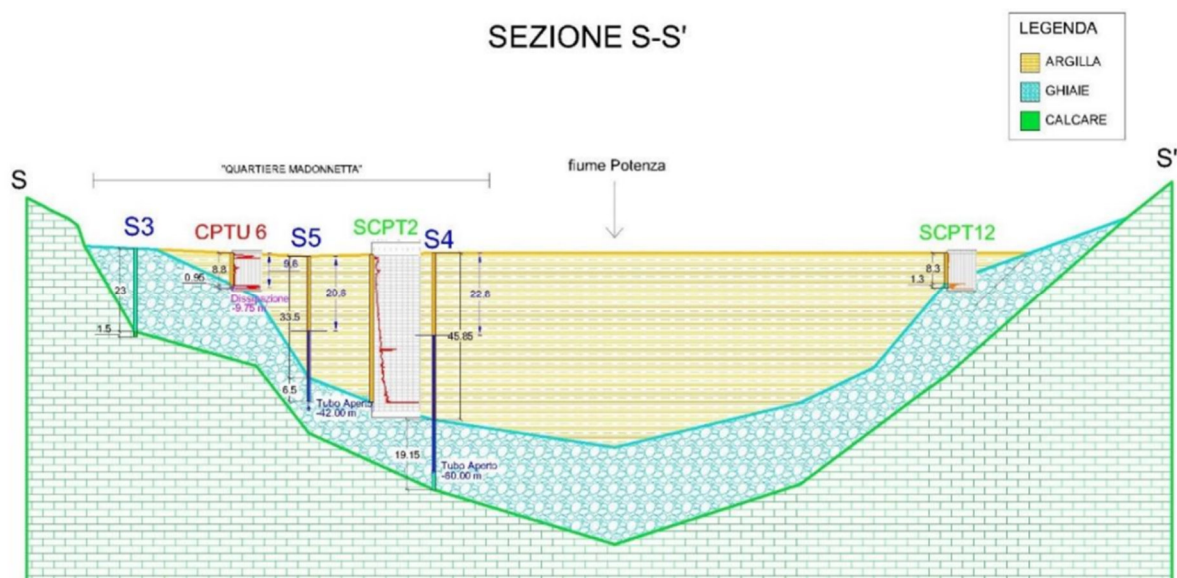

Figure 64. Geological cross section of the Madonnetta district for the implementation of the model for subsidence prediction (modified from Lenci, 2021).
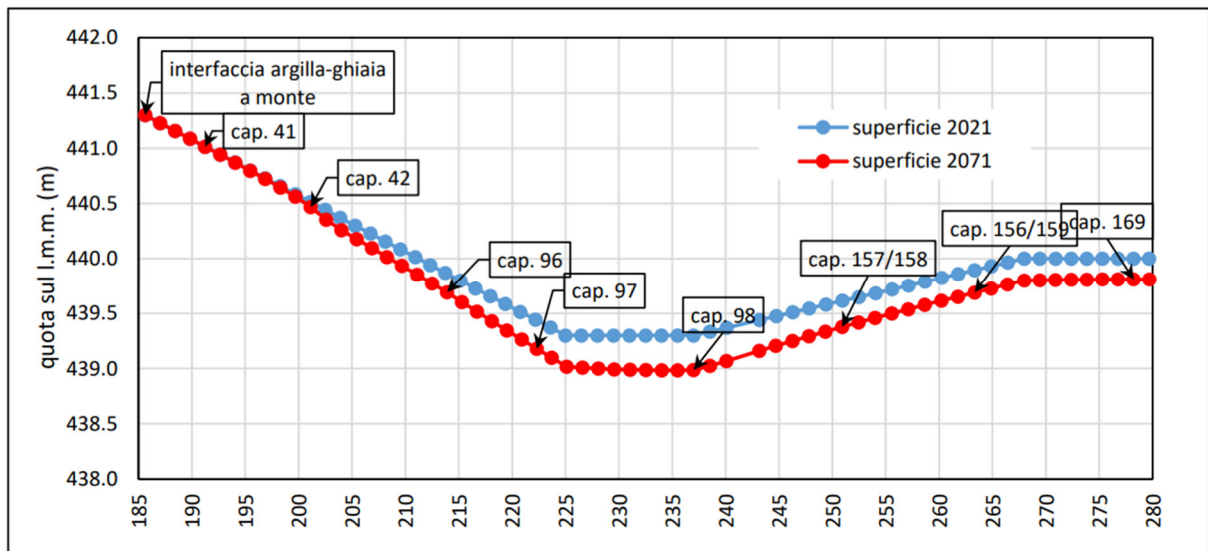
Figure 65. Vertical displacement prediction for the year 2071 (modified from Lenci, 2021).

Since the data about piezometers S5 and S4 cover a larger period, from 18/06/2021 to 26/09/2022, it is possible to notice the seasonal recharge of which the aquifer is subjected, starting in November and finishing in June, before dropping again to lower levels.

For the piezometer PZ1 the curve of the water head was made on the base of data recorded every two minutes, covering the period 21/07/2022-26/09/2022. The curve presents the typical fast response behaviour of a highly permeable aquifer, made of a decreasing trend during the summer months when the aquifer is not fed by rainfalls and followed by a rapid increase starting in September linked to heavy precipitations. Concurrently, the tracer tests have revealed permeability values around 10^{-1} cm/s for the gravel layer as expected for coarse materials. This aspect is strictly linked to the groundwater drainage system since it shows a high hydraulic gradient between S5 and S4 that drives the water displacement. The rise of electric conductivity detected in S4 and S5 after the injection of the tracer (sodium salt) in PZ1 confirm the N-S drainage direction. The shape of the curve of the tracer concentration can be due to the layer made of coarse material between S4 and S5 or just to the small quantity of tracer in relation to the water amount.

These data support the hypothesis of the presence of a preferential drainage path resulting from the hydraulic gradient between S5-S4 and following the direction of the normal fault which affects directly the permeability of the layers and the groundwater circulation. The groundwater levels monitored during the field surveys of 2022 reflect the piezometric

66

geometry of the area. The level in PZ1, S5 and S4 (Figure 52) highlights the occurrence of a water drainage in direction of S4 which remains the lowest piezometric area. Piezometer S16 is located in proximity of PZ1 and shows similar values (Table 9). The piezometers S10 and S18 are located respectively to the West and East of the depression zone show larger groundwater levels promoting the water drainage towards S4-S5 direction.

As support to the relation between the process of subsidence and the piezometric level variations, Figure 66. Groundwater level variation and displacement of a point provided by InSAR technology (Bonì, 2022). shows the groundwater depth variation in the piezometer S10 (Figure 62) and the displacement of an InSAR monitored point. By observing qualitatively, the curves it is possible to state a strong correlation that links the piezometric surface drop and the displacement rate measured with the satellite (Bonì, 2022).
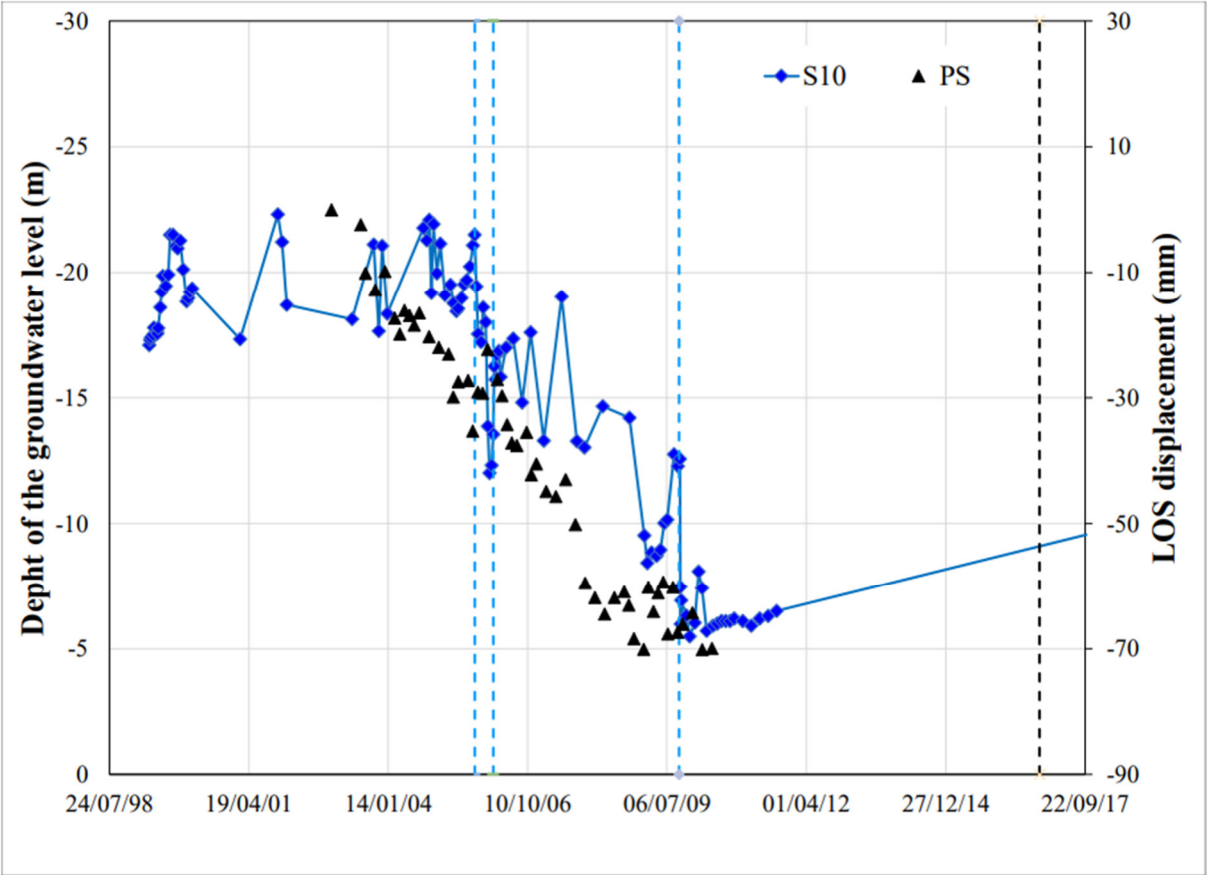

Figure 66. Groundwater level variation and displacement of a point provided by InSAR technology (Bonì, 2022).

The investigation of the hydrogeological condition, together with the geological study, underlines a complex geological condition that directly affects the underground

hydrodynamic of the area of interest. The geological study results as a fundamental support for driving the geotechnical research and modelling and in elaborated geological environments. The permeability values that result from the calculation can be adopted for geotechnical evaluations to upgrade the accuracy of the estimation of the clay compaction process.

7. Conclusions and future remarks

This thesis shows the implementation of a hydrogeological model that is featured by a complex groundwater pattern in the Madonnetta district. The geological set up of the area and the presence of a normal fault affect the water flux direction and velocity. A key role in the hydrodynamic scheme is played by the gravel layer that accommodates an intense circulation of water thanks to its elevate permeability. The integration of the hydrogeological investigation of the area of study with the piezometric level measurements and the tracer test has provided a relevant contribute to understand the principal water drainage directions and velocity. In addition, the analysis of the precipitations has provided a further insight for a wider understanding of the aquifer recharge mechanisms. These aspects seem fundamental to achieve a complete evaluation of the consolidation processes which was studied with a geotechnical model based on the results of soil samples tests and so completely detached from the hydrogeological condition. Integrating that model with parameters obtained from in-situ tests and direct measurements, such as permeability and filtration velocity of water, constitute a strong upgrade of the geotechnical model of the subsidence process which has shown a strong relationship with the piezometric oscillations, and the water drainage patterns.

8.   References

Bagheri-Gavkosh, M., Hosseini, S. M., Ataie-Ashtiani, B., Sohani, Y., Ebrahimian, H., Morovat, F., & Ashrafi, S. (2021). Land subsidence: A global challenge. *Science of The Total Environment*, *778*, 146193.

Barchi, M., Bernasconi, A., Brozzetti, F., Lavecchia, G., Menichetti, M., Minelli, G., Nardon, S., & Pialli, G. (1993). Joint distribution in a fractured carbonate reservoir in the Umbria-Marche anticlines (Central Italy). In *Generation, Accumulation and Production of Europe's Hydrocarbons III* (pp. 209–217). Springer.

Boni, Bono, Capelli (1987). Schema idrogeologico dell'Italia centrale. *Società Geologica Italiana.*

Bozzano, F., Esposito, C., Franchi, S., Mazzanti, P., Perissin, D., Rocca, A., & Romano, E. (2015). Understanding the subsidence process of a quaternary plain by combining geological and hydrogeological modelling with satellite InSAR data: The Acque Albule Plain case study. *Remote Sensing of Environment*, *168*, 219–238.

Centamore, E., Cantalamessa, G., Micarelli, A., Potetti, M., Berti, D., Bigi, S., Morelli, C., & Ridolfi, M. (1991). *Stratigrafia e analisi di facies dei depositi del Miocene e del Pliocene inferiore dell'avanfossa marchigiano-abruzzese e delle zone limitrofe*.

Cresta, S., Monechi, S., & Parisi, G. (1989). Stratigrafia del mesozoico e cenozoico nell'area umbro-marchigiana. *Memorie descrittive della Carta Geologica d'italia*, *34*, 185.

Di Stefano, Cuevas-Gonzalez, Luzi, Malinverni (2022). Assessing levelling and DInSAR for deformation monitoring in seismic region. *The International Archives of Photogrammetry, Remote Sensing and Spatial Information Sciences, 43, 263-270.*

Di Stefano, F., Cabrelles, M., García-Asenjo, L., Lerma, J. L., Malinverni, E. S., Baselga, S., Garrigues, P., & Pierdicca, R. (2020). Evaluation of long-range mobile mapping system (MMS) and close-range photogrammetry for deformation monitoring. A case study of cortes de pallas in Valencia (Spain). *Applied Sciences*, *10*(19), 6831.

Fabbi, S. (2015). Geology and Jurassic paleogeography of the Mt. Primo-Mt. Castel Santa Maria ridge and neighbouring areas (Northern Apennines, Italy). *Journal of Maps*, *11*(4), 645–663.

Galdenzi, S. (2019). Monte Lago polje, a case study regarding the influence of geologic structure and degree of karstfication on groundwater drainage in the Central Apennines (Italy). *Acta Carsologica*, *48*(1).

Lenci, S. (2021). *Relazione inerente alla ricerca scientifica relativa avente ad oggetto lo studio della perimetrazione del quartiere "Madonnetta" sito nel comune di Pioraco (MC).*

Meletti, C., Stucchi, M., Akinci, A., Faccioli, E., Gasperini, P., Malagnini, L., Montaldo, V., &
Valensise, G. (2004). *Redazione della Mappa di Pericolosità Sismica prevista
dall'Ordinanza PC del 20 marzo 2003, n. 3274, All. 1 Rapporto Conclusivo*.

Nanni (1991). Caratteri idrogeologici delle Marche. *L'ambiente Fisico delle Marche; SECLA srl:
Florence, Italy.*

Paggi, S., Pistoiesi, E., Mazza, D., Curatolo, A., & Di Girolamo, R. (2017). *Microzonazione
Sismica di Livello 3 del Comune di Pioraco ai sensi dell'Ordinanza del Commissario
Straordinario n. 24 registrata il 15 maggio 2017 al n. 1065*.

Reddish, Whittaker (2012). Subsidence: occurrence, prediction and control.

Tazioli, Aquilanti, Clementi, Marcellini, Palpacelli, Vivalda (2016). Hydraulic contacts
identification in the aquifers of limestone ridges: tracer tests in the Montelago pilot
area (Central Apennines). Acque Sotterranee-Italian Journal of Groundwater, 5(2).